



UNIVERSIDAD DE INVESTIGACIÓN DE TECNOLOGÍA EXPERIMENTAL YACHAY

Escuela de Ciencias Físicas y Nanotecnología

TÍTULO: Numerical Study of the Chaotic Inflationary Model with a Step

Trabajo de integración curricular presentado como requisito para
la obtención del título de Físico

Autor:

Vega Pallo Jonathan Javier

Tutor:

Ph.D. Rojas Cely Clara Inés

Urququí, diciembre 2022

Urcuquí, 22 de diciembre de 2022

**SECRETARÍA GENERAL
ESCUELA DE CIENCIAS FÍSICAS Y NANOTECNOLOGÍA
CARRERA DE FÍSICA
ACTA DE DEFENSA No. UITEY-PHY-2022-00023-AD**

En la ciudad de San Miguel de Urcuquí, Provincia de Imbabura, a los 22 días del mes de diciembre de 2022, a las 14:30 horas, en el Aula S_CAN de la Universidad de Investigación de Tecnología Experimental Yachay y ante el Tribunal Calificador, integrado por los docentes:

Presidente Tribunal de Defensa	Dr. COSENZA MICELI, MARIO GIUSEPPE , Ph.D.
Miembro No Tutor	BANDA BARRAGAN, WLADIMIR EDUARDO
Tutor	Dra. ROJAS CELY CLARA INES , Ph.D.

Se presenta el(la) señor(ita) estudiante **VEGA PALLO, JONATHAN JAVIER**, con cédula de identidad No. **0503991911**, de la **ESCUELA DE CIENCIAS FÍSICAS Y NANOTECNOLOGÍA**, de la Carrera de **FÍSICA**, aprobada por el Consejo de Educación Superior (CES), mediante Resolución **RPC-SO-39-No.456-2014**, con el objeto de rendir la sustentación de su trabajo de titulación denominado: **Numerical Study of the Chaotic Inflationary Model with a Step**, previa a la obtención del título de **FÍSICO/A**.

El citado trabajo de titulación, fue debidamente aprobado por el(los) docente(s):

Tutor	Dra. ROJAS CELY CLARA INES , Ph.D.
--------------	------------------------------------

Y recibió las observaciones de los otros miembros del Tribunal Calificador, las mismas que han sido incorporadas por el(la) estudiante.

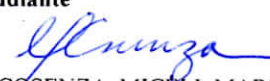
Previamente cumplidos los requisitos legales y reglamentarios, el trabajo de titulación fue sustentado por el(la) estudiante y examinado por los miembros del Tribunal Calificador. Escuchada la sustentación del trabajo de titulación, que integró la exposición de el(la) estudiante sobre el contenido de la misma y las preguntas formuladas por los miembros del Tribunal, se califica la sustentación del trabajo de titulación con las siguientes calificaciones:

Tipo	Docente	Calificación
Tutor	Dra. ROJAS CELY CLARA INES , Ph.D.	10,0
Miembro Tribunal De Defensa	BANDA BARRAGAN, WLADIMIR EDUARDO	9,7
Presidente Tribunal De Defensa	Dr. COSENZA MICELI, MARIO GIUSEPPE , Ph.D.	10,0


Lo que da un promedio de: **9.9 (Nueve punto Nueve)**, sobre 10 (diez), equivalente a: **APROBADO**

Para constancia de lo actuado, firman los miembros del Tribunal Calificador, el/la estudiante y el/la secretario ad-hoc.


VEGA PALLO, JONATHAN JAVIER
Estudiante


Dr. COSENZA MICELI, MARIO GIUSEPPE , Ph.D.
Presidente Tribunal de Defensa


Dra. ROJAS CELY CLARA INES , Ph.D.
Tutor


BANDA BARRAGAN, WLADIMIR EDUARDO
Miembro No Tutor


CIFUENTES TAFUR, EVELYN CAROLINA
Secretario Ad-hoc

Autorización de Publicación

Yo, **Jonathan Javier Vega Pallo**, con cédula de identidad **0503991911**, declaro que las ideas, juicios, valoraciones, interpretaciones, consultas bibliográficas, definiciones y conceptualizaciones expuestas en el presente trabajo; así como, los procedimientos y herramientas utilizadas en la investigación, son de absoluta responsabilidad de el autor del trabajo de investigación curricular. Así mismo, me acojo a los reglamentos internos de la Universidad de Investigación de Tecnología Experimental Yachay.

Urququí, enero 2023

Jonathan Javier Vega Pallo

CI: 0503991911

Autorización de Publicación

Yo, **Jonathan Javier Vega Pallo**, con cédula de identidad **0503991911**, cedo a la Universidad de Tecnología Experimental Yachay, los derechos de publicación de la presente obra, sin que deba haber un reconocimiento económico por este concepto. Declaro además que el texto del presente trabajo de titulación no podrá ser cedido a ninguna empresa aditorial para su publicación u otros fines, sin contar previamente con la autorización escrita de la Universidad.

Asimismo, autorizo a la Universidad que realice la digitalización y publicación de este trabajo de integración curricular en el repositorio virtual, de conformidad con lo dispuesto en el Art. 144 de la Ley Orgánica de Educación Superior.

Urcuquí, enero 2023

Jonathan Javier Vega Pallo

CI: 0503991911

Abstract

The theory of cosmological inflation arises in order to solve the problems and inconsistencies that the classical theory of the Big Bang presented. This theory states that there was a period of exponential growth of the Universe for a very short period of time. Cosmic inflation models are of great importance to solve the problems of the initial conditions that describe the evolution of the Universe. Despite a large number of proposed models, some of these, such as the chaotic or tachyon potential, are often ignored due to the poor approximation they have to cosmological quantities, such as the spectral indices n_s and r . The introduction of a step potential within these potentials generates oscillations in the scalar power spectrum that improves the fits to the observational data obtained by space telescopes, at angular momentum $l = 22$ and $l = 40$ of the angular power spectrum. The numerical analysis made on each of the components that make up the chaotic potential with a step shows the different behaviors that these variables have. The spectral indices calculated for the best fit model studied, show a good approximation to those obtained observationally.

Keywords: Cosmological inflation, chaotic potential, scalar power spectrum, angular power spectrum

Resumen

La teoría de la inflación cósmica surge con el fin de solucionar los problemas e inconsistencias que presentaba la teoría clásica del Big Bang. Esta teoría afirma que hubo un periodo de crecimiento exponencial del Universo durante un periodo de tiempo muy corto. Los modelos de inflación cósmica son de gran importancia para resolver los problemas de las condiciones iniciales que describen la evolución del Universo. A pesar de la gran cantidad de modelos propuestos, algunos de estos, como el potencial caótico o de taquiones, suelen ser ignorados debido a la mala aproximación que pueden tener en las cantidades cosmológicas como los índices espectrales n_s y r . La introducción de un potencial escalón dentro de estos potenciales genera oscilaciones en el espectro de potencia escalar que mejora los ajustes de los datos observacionales obtenidos por los telescopios espaciales, en los momentos angulares $l = 22$ y $l = 40$ del espectro de potencias angulares. El análisis numérico hecho sobre cada uno de los componentes que conforman el potencial caótico con un escalón, muestra los distintos comportamientos que tienen estas variables. Los índices espectrales calculados para el modelo de mejor ajuste, muestran una buena aproximación a los obtenidos observacionalmente.

Palabras Clave: Inflación cosmológica, potencial caótico, espectro de potencia escalar, espectro de potencia angular.

Acknowledgements

I want to infinitely thank my advisor, Ph. D. Clara Rojas for trusting me and helping me with her time and patience during this thesis work. Thank you very much for orienting me and guiding me towards a new area that will open hundreds of doors in my professional life.

I want to thank my parents, Abelardo, María, Olga and Sergio, with all my heart, for being the fundamental pillars so that my goal of being a professional has been fulfilled. To my brothers, Edison, Karla and Melany, for being an engine to keep me striving. To Deysi, for being my great moral support throughout my career.

I cannot forget my great friends, my second family, who accompanied me during my career at Yachay: Jorge, Harvey, Gustavo, Jefferson, Mirian, Margarita, Ivette, Alexa, Daniela, Jennifer, Camila and many more. Thank you for making the University another place like home.

I would like to thank all the members who made up and make up the Club de Bienestar Animal (CBA), for giving me the opportunity to serve the university community in extracurricular matters.

Finally, thank you Yachay Tech for all the experiences provided from my beginnings, until this last semester of my career. Thanks to all the people and teachers I was able to meet during all this time, my best wishes to everyone.

Contents

List of Figures	xiv
List of Tables	xvi
1 Introduction	1
1.1 General Overview	1
1.2 General and Specific Objectives	2
2 Theoretical Background	3
2.1 The Big Bang Theory	3
2.2 Fine-Tuning Problems	6
2.2.1 Flatness Problem	7
2.2.2 Horizon Problem	7
2.3 Inflation Theory	9
2.4 Amount of Inflation	10
2.4.1 Inflation as a solution to Flatness Problem	10
2.4.2 Inflation as a solution to Horizon Problem	11
2.5 Scalar Field in Cosmology	11
2.6 Equations of motion	13
3 Methodology	15
3.1 Slow-Roll Approximation	15
3.1.1 Relation Between Slow-Roll and Inflation	16
3.2 Cosmological Perturbations in the Geometry of the Universe	17
3.2.1 Quantum Perturbations	19
3.2.2 Scalar perturbations equation	21
3.2.3 Power Spectrum for Perturbations	25
3.2.4 The Power law case	25
3.3 Cosmological Inflation Models	26

3.3.1	Chaotic Inflationary Model with a Step	27
4	Results and Discussion	29
4.1	Numerical Analysis of the Chaotic Potential without a step	29
4.2	Numerical Analysis of the Chaotic Potential with a step	31
4.2.1	Numerical analysis of the chaotic potential with values outside the limits	31
4.2.2	Numerical analysis of the chaotic potential with a step with a combination between values that are outside and inside the limits	32
4.2.3	Numerical analysis of the chaotic potential with the lower and upper limit values	32
4.2.4	Numerical analysis of the potential with values within the limits	32
5	Conclusions & Outlook	41
A	Short Appendix 1 Heading for the Table of Contents	43
	Bibliography	47

List of Figures

2.1	Temperature fluctuations measured in the CMB radiation using COBE in 1992, WMAP in 2003 and Planck in 2013 ¹	8
3.1	Representation of an inflation potential. The accelerated expansion of the Universe occurs when the potential energy of the field, V_ϕ , is vastly greater than its kinetic energy ($\frac{\dot{\phi}^2}{2}$). Inflation ends when $V_\phi \approx \frac{\dot{\phi}^2}{2}$. CMB fluctuations are created by quantum fluctuations, δ_ϕ , about 60 e-folds before the end of inflation ²	16
3.2	The CMB angular power spectrum corresponding to the best fit values of the inflationary models for the WMAP seven-year. The dark dots with its respective error represent the data obtained by WMAP seven-year. The blue line and the dashed green line corresponds corresponds to the chaotic potential without and with a step data ³ . The red ellipses show the fit that occurs near the multipolar moments $l = 22$ and $l = 40$, due to the step in the chaotic potential.	26
3.3	The scalar field potential for the chaotic model for $m = 7.5 \times 10^{-6} M_{pl}$. Left: without a step. Right: with a step with $c = 0.200$, $d = 0.0311$ and $\phi_{step} = 14.670$	27
4.1	Scalar power spectrum for the chaotic potential without the step. The red horizontal line represents the approximate value that the potential must approach for it to be considered a valid model. The parameters used for both the blue color potential and the green color potential are exactly the same except for the value of m ; see Table (4.1). The difference presented by $m = 6.5 \times 10^{-6} M_{pl}$ and $m = 7.5 \times 10^{-6} M_{pl}$ seems to result in a vertical displacement of the potential.	30
4.2	Scalar power spectrum for values of c , ϕ_{step} and d that are outside the limits established in Table (4.2). The values considered for the blue color spectrum are above the limits, while for the purple color spectrum the values of the parameters are below the restrictions.	33
4.3	Scalar power spectrum for combinations of values that are inside and outside the limits. Left: where c is the only parameter whose value is outside the limits. Right: choosing c and d with values outside the restrictions. In both cases the oscillations with blue color have a value of $m = 7.5 \times 10^{-6} M_{pl}$ while for the oscillations with green color a value $m = 6.5 \times 10^{-6} M_{pl}$ was used. The red line shows the final trend that a model must follow in order to be considered valid.	33

4.4	Scalar spectrum for the chaotic potential with the parameters defined in Table (4.5). <i>Left</i> : lower limit. <i>Right</i> : upper limit. In both cases, m is the only parameter varied in the blue ($m = 7.5 \times 10^{-6}$) and purple ($m = 6.5 \times 10^{-6}$) graphs. As in the previous cases, the red line represents the trend that the studied potential should follow.	35
4.5	Scalar power spectrum for different values of c . The oscillatory behavior in this case shows an increase in the amplitude of the wave as c increases as well.	36
4.6	Scalar power spectrum for different values of ϕ_{step} . The oscillatory frequency of the blue color spectrum is greater than purple and green color spectra.	37
4.7	Spectrum of scalar powers for different values of d . The behavior of these oscillations looks contrary to those obtained by the previous spectra.	38
4.8	The scalar power spectrum of the best fit found for the chaotic potential with a step. The graph shows oscillations and its final value tends to have a value of 2.2×10^{-9} . The range of the wavenumber is smaller in relation to the previous cases.	40

List of Tables

2.1	Temperature and density of the Universe from the singularity to the present.	3
4.1	Parameters used for the graphic representation of Fig. (4.1). The cosmological values n_s and r are obtained for this case.	29
4.2	Range of values that can be considered for the different parameters present in the power law case and the chaotic potential. These limits taken from Dhiraj's ³ article were modified considering that there are more combinations of values that the variables of the chaotic potential with a step can have.	31
4.3	Values used in the parameters of the potentials shown in Fig. (4.2)	32
4.4	Parameters used to obtain the figure of the power spectrum in Fig. (4.3), with m being the only one quantity that varies in the graph on the left and right. The numbers in bold represent the chosen quantities that are outside the limits.	34
4.5	Upper and lower limit of the potential parameters calculated with the Markov Chain Monte-Carlo method. The values of n_s and r were obtained for both limits	34
4.6	Values considered for the parameters of the step potential. The variation occurs over the value c , while the rest of the quantities remain constant. The power law cases (n_s and r) were calculated	35
4.7	Values considered for the step potential parameters. The variation of ϕ_{step} between the second and third value is smaller in relation to the first.	36
4.8	Different values considered for parameter d . The quantities n_s and r obtained for this case are shown	38
4.9	Values of the parameters that best fit the observational data from space telescopes. The quantities n_s and r obtained for this fit are shown.	39
4.10	Experimental and theoretical values obtained for n_s and r	39

Chapter 1

Introduction

1.1 General Overview

How our Universe came about and how it has evolved are two of the great questions that humans have asked themselves throughout history. Although there have been many theories that seem to give an answer to these two questions, the one that has convinced scientists most, due to the observational evidence found, is the so-called Big Bang theory.

In 1915, Albert Einstein published his famous theory of General Relativity in which he provides a new tool for understanding the dynamics of the Universe. The first person to use the equations that Einstein had proposed was the Russian scientist Alexander Friedman in 1920, whose objective was to show that the Universe could not be static; it either expanded or compressed. Later, in 1927, the Belgian priest George Lemaitre would use the mathematics of General Relativity to propose a Universe in constant expansion, which he called the Big Bang. The Big Bang theory was born with the aim of giving an explanation to the origin and expansion of the Universe from a hot spot, called a singularity, where all matter and the space in which it moves were formed. Currently, the observations made by Edwin Hubble in 1927 discovered that galaxies are moving away from each other, and the discovery of the microwave background radiation (CMB) in 1965, support Lemaitre's theory of birth and subsequent expansion of the universe. Although the acceptance of the Big Bang, as a solution to the problem of the origin of the Universe, has been widely accepted by the scientific community, it presents issues such as the problem of the horizon and flatness, which have only been resolved through cosmological inflation. The cosmological inflation was proposed by the physicist Alan Guth in 1981. The main objective of this approach is to give an explanation to the anisotropies observed in the CMB and the large-scale planar structure of the Universe. Many different inflationary models have been proposed, each with different underlying physics and motivation. Currently, testing the validity of each model is an active area of investigation within inflation.

1.2 General and Specific Objectives

- The main objective of this paper is to numerically analyze the scalar perturbation equations of the chaotic inflationary model with a step, in order to understand the behavior of the height, c , location/coordinate, ϕ_{step} , and width, d , parameters that characterize this step potential. The specific objectives of this work are to:
 - Determine the influence of the step potential on the chaotic potential.
 - Establish new upper and lower limits of the parameters c , ϕ and d , of the spectral index n_s and of the scalar-to-tensor ratio r .
 - Analyze the different oscillatory behaviors that the chaotic potential with a step presents with different variations in the values of its parameters.
 - Find the best combination of values in the parameters of the chaotic potential whose results in the spectral index and scalar-to-tensor ratio are the closest to the results obtained experimentally by the Planck space telescope.

The analysis begins in Chapter 2, where the theoretical background necessary for a correct understanding of this work is detailed. Then, Chapter 3 shows the methodology used, where the calculations performed to obtain the equations of the scalar and tensor perturbations are shown, as well as the spectral indices and the tensor-to-scalar ratio. Finally, Chapter 4 shows the scalar power spectrum obtained for all the cases analyzed, each one with its respective values of spectral index n_s and tensor-to-scalar ratio r .

Chapter 2

Theoretical Background

2.1 The Big Bang Theory

The idea of a large-scale homogeneous and isotropic Universe, that is, a similar Universe in all parts and directions, arises from different measurements that have been made with different telescopes. This postulate states that there was a great explosion about 13.8 billion years ago, when the amount of matter was zero and the density and temperature were infinite. Table (2.1) shows the evolution of the Universe from the Big Bang to the present. An expanding or contracting homogeneous and isotropic Universe can be described by the Friedmann-Lamaître Robertson-Walker (FLRW) metric, which is an exact solution to the Einstein field equations. Under certain circumstances the initial metric can be written as:

$$ds^2 = c^2 dt^2 - h_{ij} dx^i dx^j, \quad (i, j = 1, 2, 3) \tag{2.1}$$

Time [s]	Temperature [°C]	Density [kg/m ³]	Features
0	∞	∞	The size of the Universe is zero
0.01	1 × 10 ¹¹	—	Energy dominates over radiation
2	1 × 10 ¹⁰	1 × 10 ⁸	Particles and antiparticles begin to form
180	1 × 10 ⁹	—	Hydrogen and helium begin to form
12000	—	—	1/4 of the Universe is Helium
3.15 × 10 ¹¹	1 × 10 ⁴	1 × 10 ⁻¹⁷	Matter dominates over radiation
Now	-270	1 × 10 ⁻²⁷	Temperature we currently measure

Table 2.1: Temperature and density of the Universe from the singularity to the present.

where h_{ij} are the space-time coordinates (t, r, θ, ϕ) . From Eq. (2.1) the standard form of the FLRW metric can be obtained, which has the following form:

$$ds^2 = -dt^2 + a(t)^2 \left(\frac{dr^2}{1 - kr^2} + r^2 d\theta^2 + r^2 \sin^2 \theta d\phi^2 \right). \quad (2.2)$$

This equation is formulated in polar coordinates, where $a(t)$ is the cosmic time-dependent scale factor that describes the expansion of the Universe. The spatial curvature is represented by the letter k , which is a constant that can only take 3 values: $k = 1$, $k = -1$, and $k = 0$. When $k = 1$ the Universe describes a positive spatial curvature, if $k = -1$ the Universe curvature is negative, and for $k = 0$ the spatial curvature is flat; Measurements currently taken show that our Universe has a value of k very close to 0, in other words our universe has a flat spatial geometry (Euclidean geometry). For this reason, it is convenient to normalize $a(t)$ to get a value equal to 1 at current times.

A comoving point can be defined as one that moves together with the expansion of the Universe. The measured distance from our place of location to a random comoving point can be represented by the formulation:

$$r(t) = x a(t), \quad (2.3)$$

where x is known as the comoving distance. The conformal time is another useful quantity that is used very often in cosmology, whose physical expression is given as:

$$d\tau = \frac{dt}{a(t)}. \quad (2.4)$$

In the area of cosmology, a conventional notation is considered where the speed of light (c) has a value equal to 1, so all speeds will be measured around this c value²; in this work we consider all equations with this value. Other quantities such as the Planck mass (M_{pl}), Plack time (T_{pl}), and the Plack length (L_{pl}) have the values of 4.342×10^{-6} g, 2.70×10^{-43} s, and 8.10×10^{-33} cm respectively. In General Relativity, the evolution and space-time properties of the Universe are described by Einstein's field equations*⁴, which are mathematically described as:

$$R_{\mu\nu} - \frac{1}{2}g_{\mu\nu}R - g_{\mu\nu}\Lambda = \frac{8\pi}{M_{pl}^2}T_{\mu\nu}, \quad (2.5)$$

where $R_{\mu\nu}$ and R are the Ricci tensor and scalar respectively, G is Newton's universal gravitation constant, $G_{\mu\nu}$ is the curvature tensor, and Λ is Einstein's gravitational cosmological constant. The metric tensor ($g_{\mu\nu}$), that describes the entire geometric structure of space-time, and the energy-momentum tensor ($T_{\mu\nu}$), that describes the configuration of

*The Einstein field equations are a set of 10 equations proposed by the German scientist Albert Einstein, which describe gravity as a deformation of space-time produced by its interaction with matter and energy.

matter and energy of the Universe⁵, are represented by:

$$g_{\mu\nu} = \begin{pmatrix} -1 & 0 & 0 & 0 \\ 0 & \frac{a^2(t)}{1-kr^2} & 0 & 0 \\ 0 & 0 & a^2(t)r^2 & 0 \\ 0 & 0 & 0 & a^2(t)r^2 \sin^2 \theta \end{pmatrix}, \quad (2.6)$$

$$T_{\nu}^{\mu} = \begin{pmatrix} \rho & 0 & 0 & 0 \\ 0 & -p & 0 & 0 \\ 0 & 0 & -p & 0 \\ 0 & 0 & 0 & -p \end{pmatrix}, \quad (2.7)$$

For simplicity, we can write Eq. (2.5) in another way, multiplying the entire expression by the inverse of the metric tensor, so we will only have an equation with scalar terms with the form:

$$R + 4\Lambda = -\frac{8\pi}{M_{pl}^2}T, \quad (2.8)$$

It can be seen that within the equation we have a T that would represent an energy-momentum scalar. If we solve for R from Eq. (2.8) and replace it in Eq. (2.5) we will obtain:

$$R_{\mu\nu} + g_{\mu\nu}\Lambda = \frac{8\pi}{M_{pl}^2} \left(T_{\mu\nu} - \frac{1}{2}g_{\mu\nu}T \right). \quad (2.9)$$

Writing this equation this way, with the dependence on the tensor and the energy-momentum scalar on the right hand side of Eq. (2.9), makes calculations easier. Due to the homogeneity and isotropy of the Universe, $T_{\mu\nu}$ can be written as an expression of a perfect fluid as follows:

$$T^{\mu\nu} = (\rho + p)U^{\mu}U^{\nu} - g^{\mu\nu}p. \quad (2.10)$$

where ρ represents the energy density, p is the internal pressure, and U is the four-speed vector. In a universe that follows established cosmological principles, the vector U will only have the time component:

$$U^{\mu} = (1, 0, 0, 0). \quad (2.11)$$

The energy-momentum scalar will also have dependence on ρ and p :

$$T = \rho - 3p, \quad (2.12)$$

Substituting Eqs. (2.6), (2.7) and (2.12) in Eq. (2.9), we obtain a spatial and temporal solution to the Ricci tensor that depends on the scale factor. The spatial part of Einstein's field equations will be the expression:

$$\frac{\ddot{a}}{a} + 2\frac{\dot{a}^2}{a^2} + 2\frac{K}{a^2} = \frac{4\pi}{M_{pl}^2}(\rho - p) + \Lambda, \quad (2.13)$$

While the temporary part will be:

$$\frac{\ddot{a}}{a} = -\frac{4\pi}{3M_{pl}^2}(\rho + 3p), \quad (2.14)$$

If we substitute Eq. (2.14) into Eq. (2.13), we will obtain a single equation:

$$H^2 = \left(\frac{\dot{a}}{a}\right)^2 = \frac{8\pi}{3M_{pl}^2}\rho - \frac{k}{a^2}. \quad (2.15)$$

This last formulation is known as the Friedmann equation, which represents a solution to the dynamic evolution of the Universe. As mentioned above, the value of k is very close to zero for our current Universe, so Eq. (2.15) would be:

$$\left(\frac{\dot{a}}{a}\right)^2 = H^2 = \frac{8\pi}{3M_{pl}^2}\rho. \quad (2.16)$$

where $H = \dot{a}/a$ is the Hubble parameter. The continuity (or fluid) equation can be obtained by conserving the energy-momentum tensor:

$$\dot{\rho} + 3H(\rho + p) = 0, \quad (2.17)$$

The Eq. (2.17) can also be written as:

$$a \frac{d\rho}{da} = -3(\rho + p). \quad (2.18)$$

The Friedmann equation (2.16) can also be represented terms of the density parameter Ω

$$\Omega(t) - 1 = \frac{k}{a^2 H^2}, \quad (2.19)$$

where $\Omega(t) = \rho/\rho_c$. Furthermore, the critical density (ρ_c) is defined by the Hubble parameter and the Planck mass:

$$\rho_c = \frac{3H^2 M_{pl}^2}{8\pi}. \quad (2.20)$$

For a spatially flat geometry, $k = 0$, Eq. (2.19) will show that Ω must be equal to 1. If Eq. (2.18) is solved, we obtain:

$$\rho \propto a^{-3(1+p)}. \quad (2.21)$$

where it can be analyzed that the evolution of the Universe is going to occur in terms of the scale factor, in addition to the relationship of the domain of matter, radiation and vacuum at different epochs of the Universe.

2.2 Fine-Tuning Problems

Despite the fact that the Big Bang theory describes in an acceptable way the evolution and dynamics of the Universe on a large scale, it presents some errors that cannot be solved by themselves, in this work we only mention the two most popular problems of the theory of the Big Bang.

2.2.1 Flatness Problem

The flatness problem is also considered to be the biggest drawback in the classical Big Bang theory⁶. Considering Eq. (2.19), the term $a^2H^2(= \dot{a})$ always decreases⁴ with respect to time. Current cosmological observations, based on the standard model, suggest that the present value of Ω is:

$$\Omega_0 \sim 1.0007 \pm 0.0037. \quad (2.22)$$

The subscript 0 represents the quantities measured at the current time and for the case of the density parameter, Eq. (2.22), it has a value very close to unity. A small variation on this value results in a radical change in the curvature of space. The tuning problem arises because in early times Ω must be set to 1. However, this is not completely convincing because all standard cosmology models start with $\Omega = 1$ ⁷. The present age of the Universe is estimated to be $t_0 \approx 13.787$ Gyrs¹. If we want to know the correct spatial geometry for an arbitrary time (t), we can use the expression:

$$|\Omega - 1| = |\Omega_0 - 1| \frac{t}{t_0}. \quad (2.23)$$

Using the values t_0 and Ω_0 expressed above we will obtain for:

- $t \approx 10^{-43}$ seconds

$$|\Omega - 1| \leq 10^{-64}, \quad (2.24)$$

- $t \approx 1$ second

$$|\Omega - 1| \leq 10^{-16}, \quad (2.25)$$

- $t \approx 10^{13}$ seconds

$$|\Omega - 1| \leq 10^{-3}. \quad (2.26)$$

The values obtained in Eqs. (2.24), (2.25) and (2.26) show us that for early times $|\Omega - 1|$ has to be fine-tuned extremely close to zero¹ to reach the value shown in Eq. (2.22).

2.2.2 Horizon Problem

This issue is one of the important details that the CMB presents and the classical Big Bang theory cannot explain. The CMB appeared as an extremely uniform radiation, however it is not explained how two regions that are too far apart from each other, with independent evolutions, present exactly the same temperature. The photons present in an early Universe could not travel freely through space due to the interaction they had with the other components present. Later, with a universe with a lower density and temperature, the protons and electrons began to then connect to hydrogens atoms with a neutral charge, which is known as recombination, where the photons finally began to move freely across the Universe. This event on photons is known as the decoupling time and it occurred at an approximate temperature of $T_{dec} \approx 0.3$ eV at red-shift $z_{rec} \approx 1100$ ¹. The spherical surface seen in Fig. (2.1) is also known as the

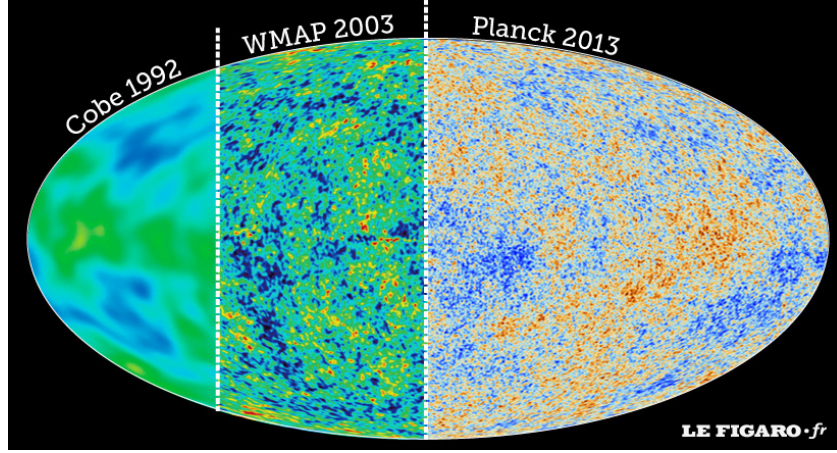


Figure 2.1: Temperature fluctuations measured in the CMB radiation using COBE in 1992, WMAP in 2003 and Planck in 2013¹

surface of the last scattering. This scattering is thought to have occurred about 380,000 years after the Big Bang. The approximate angular diameter distance of the Universe for $\Omega = 1$ is represented by:

$$d_A(z) = \frac{r(z)}{1+z}, \quad (2.27)$$

where $r(z)$ is the proper distance, for an observer located in a redshift, and is given by:

$$r(z) = \int_{t_{\text{em}}}^{t_0} \frac{dt}{a(t)} = \int_{a_{\text{em}}}^1 \frac{da}{a^2} H(a) = \int_0^z \frac{dz}{H(z)}. \quad (2.28)$$

For an adequate analysis of this problem, the quantity $\Omega = \Omega_m$ would represent the value taken by the density parameter during the era of matter domination. Taking this into account, we can approximate the $H(z)$ of Eq. (2.28) as:

$$H(z) \approx \sqrt{\Omega_m H_0^2 (1+z)^3}, \quad (2.29)$$

Inserting Eq. (2.29) into Eq. (2.28)

$$r(z) = \int_0^z \frac{dz}{H(z)} = \frac{1}{\sqrt{\Omega_m} H_0} \int_0^z \frac{dz}{(1+z)^{3/2}} = \frac{2}{\sqrt{\Omega_m} H_0} \left(1 - \frac{1}{\sqrt{1+z}} \right), \quad (2.30)$$

We know the condition $z_{\text{rec}} \gg 1$, so the last expression will approximate:

$$r(z) \approx \frac{2}{\sqrt{\Omega_m} H_0}, \quad (2.31)$$

With $r(z)$ obtained, the size of the observable Universe for $z = z_{\text{rec}}$ will be:

$$d_A(z) \approx \frac{2}{\sqrt{\Omega_m} H_0} \frac{1}{(1+z)}, \quad (2.32)$$

$$d_A(1100) \approx 14 \text{ Mpc}.$$

The particle horizon is the distance light has traveled from $t = 0$ to a given time t^8 . The comoving distance to the event horizon is:

$$d_{\text{hor,rec}}(z) = \int_0^{t(z)} \frac{1}{a(t)} dt = \int_z^\infty \frac{1}{H(z)} dz \approx \frac{2}{\sqrt{\Omega_m} H_0} \left[\frac{1}{\sqrt{1+z}} \right]_z^\infty \approx \frac{2}{\sqrt{\Omega_m} H_0} \frac{1}{\sqrt{1+z}}, \quad (2.33)$$

Then, the size of the particle horizon (D) will be:

$$D(z) = a(z) d_{\text{hor,rec}} = \frac{d_{\text{hor,rec}}(z)}{(1+z)}, \quad (2.34)$$

$$D(1100) \approx 0.03 \approx 2 \text{ degrees}.$$

This tells us that the regions separated by approximately 2 degrees are causally disconnected but the isotropy observed in the CMB implies that the radiation was homogeneous and isotropic within regions located on the last scattering surface¹ (see Fig. 2.1), then the question that arises is how this thermal equilibrium originates at the moment of decoupling. Currently, the CMB has the same temperature throughout the sky, this is approximately $2.726 \pm 0.001 \text{ K}^9$.

2.3 Inflation Theory

The theory of inflation is based on the accelerated exponential expansion of the Universe during a very short fraction of a second² ($\ddot{a} > 0$). This works as a complement and solution to the different problems that the Big Bang theory presents during the early Universe. If we consider the matter part, the inflationary condition¹⁰ is established:

$$p = -\frac{\rho}{3}, \quad (2.35)$$

This condition can also be expressed as:

$$\frac{d}{dt} \frac{H^{-1}}{a} < 0. \quad (2.36)$$

where $\frac{H^{-1}}{a}$, which is the comoving Hubble Length, is decreasing with respect to time¹¹. If we consider Eq. (2.14) and the expansion condition of the Universe $\ddot{a} > 0$ we obtain:

$$\ddot{a} > 0 \iff (\rho + 3p) < 0. \quad (2.37)$$

Since in standard physics the density (ρ) is a positive quantity, from Eq. (2.37) we can find the condition:

$$p < -\frac{\rho}{3}. \quad (2.38)$$

which tells us that there should be a special type of material in which its pressure is negative, but there is no type of radiation or component that fulfills this characteristic¹. The Hubble time H^{-1} and the Hubble distance cH^{-1} are two quantities of great importance, together with the Hubble parameter $H = \dot{a}/a$ that help describe the rate of expansion of the Universe at any time¹².

2.4 Amount of Inflation

The amount of inflation, also known as the number of e-foldings, is a value that can be quantified using the natural logarithm of the scale factor at the end of inflation and its value at some initial point in time.

$$N \equiv \ln\left(\frac{a_f}{a}\right) = \int_{t_f}^t H dt. \quad (2.39)$$

From this last expression, the value taken by N decreases as time passes, becoming zero at the end of the inflationary period. In sections 2.4.1 and 2.4.2 we will see how, to solve the horizon and flatness problems, the minimum amount of inflation is approximately 60 e-foldings. This value is not fixed and it varies depending on the cosmological model under study.^{13 14}

2.4.1 Inflation as a solution to Flatness Problem

The typical solution to this problem is to consider a cosmological constant Λ , with an equation of state $p = \rho$, which can be considered as a perfect fluid. A period of the universe during which $p = \rho$ is called de Sitter stage¹⁵. Analyzing this stage within the fluid equation (2.17):

$$\begin{aligned} \dot{\rho} + 3H(\rho + p) &= 0, \\ d\rho/dt + 3H(\rho - p) &= 0, \\ d\rho/dt &= 0, \\ \rho &= \text{constant}. \end{aligned} \quad (2.40)$$

This in turn tells us that the Universe is exponentially expanded:

$$a(t) \propto \exp\left(\sqrt{\frac{\Lambda}{3}}t\right). \quad (2.41)$$

With this, the condition of Eq. (2.36) is fulfilled. Let us consider a general solution where the accelerated expansion occurred, that is to say that the Hubble length decreases as time passes, so in Eq. (2.19) the value of Ω tends to the value of unity instead of moving away from it. Let t_i at the beginning of the inflation period, t_f as the end of it and N as the number of electronic folds¹, then:

$$N = \ln\left[H_I(t_f - t_i)\right]. \quad (2.42)$$

$$|\Omega - 1|_{t=t_f} \sim 10^{-60}, \quad (2.43)$$

and

$$\frac{|\Omega - 1|_{t=t_f}}{|\Omega - 1|_{t=t_i}} = e^{-2N}, \quad (2.44)$$

$$\left|\Omega(t_f) - 1\right| = e^{-2N} |\Omega(t_i) - 1|. \quad (2.45)$$

Suppose that before to inflation, the Universe was actually fairly strongly curved with:

$$|1 - \Omega(t_i)| \sim 1. \quad (2.46)$$

After a hundred e-foldings of inflation, the derivation of Ω from one would be:

$$|1 - \Omega(t_f)| \sim e^{-2N} \sim e^{-120} \sim 10^{-87}. \quad (2.47)$$

From this last equation it can be seen that e-folding must be $N \approx 60$ so that the quantity Ω_0 adapts to the value currently measured, so that Ω reaches a value very close to unity. Taking this, the problem of the large-scale flatness of the Universe seems to be solved^{1 16 15}.

2.4.2 Inflation as a solution to Horizon Problem

Inflation greatly increases the size of a region of the Universe, while keeping its characteristic scale constant, the Hubble scale (H^{-1}). Physical scales can be reduced exponentially if the expansion period lasts long enough. This would allow these scales, which have left the horizon, to re-enter the past. The problem of the horizon can be solved if we analyze how long inflation should have lasted. For this, the horizon we observe today (H_0^{-1}) was reduced during inflation to a value $\lambda_{H_0}(t_i)$ smaller than the value of the length of the horizon (H_I^{-1}) during inflation¹⁵. This is:

$$\lambda_{H_0}(t_i) = H_0^{-1} \left(\frac{a_{t_f}}{a_{t_0}} \right) \left(\frac{a_{t_i}}{a_{t_f}} \right) = H_0^{-1} \left(\frac{T_0}{T_f} \right) e^{-N} \lesssim H_I^{-1}, \quad (2.48)$$

where T_0 is the current temperature of the Universe and T_f the temperature at the end of inflation. Developing Eq. (2.48) to obtain the inequality with respect to N :

$$e^{-N} \leq \frac{H_0}{H_I} \left(\frac{T_f}{T_0} \right) \quad (2.49)$$

Applying natural logarithm:

$$N \geq \ln \left(\frac{H_0}{T_0} \right) - \ln \left(\frac{T_f}{H_I} \right) \quad (2.50)$$

Then, we get for N :

$$N \approx 67 + \ln \left(\frac{T_f}{H_I} \right) \quad (2.51)$$

With which we obtain a quantity $N \geq 60$ that would solve the horizon problem¹¹

2.5 Scalar Field in Cosmology

As we saw in previous sections, for inflation to take place we need a candidate term whose main characteristic is that of having negative pressure. There is a large number of cosmological models whose objective is to give a theoretical approximation to the observed quantities¹. The simple scalar field responsible for inflation is also called the inflaton,

ϕ . Despite the fact that scalar fields were introduced by particle physicists long before it became a field of study of great interest, they have not been discovered experimentally until now¹³. Let's analyze our candidate (ϕ) minimally coupled to gravity with a random potential ($V(\phi)$) and a Lagrangian density, \mathcal{L} .

$$S = \int d^4x \sqrt{-g} \mathcal{L} = \int d^4x \sqrt{-g} \left[\frac{1}{2} \partial_\mu \phi \partial^\mu \phi + V(\phi) \right], \quad (2.52)$$

where $\sqrt{-g} = a^3$ from Eq. (2.2). From the Euler-Lagrange equations

$$\partial^\mu \frac{\delta(\sqrt{-g} \mathcal{L})}{\delta \partial^\mu \phi} - \frac{\delta(\sqrt{-g} \mathcal{L})}{\delta \phi} = 0. \quad (2.53)$$

So we obtain:

$$\ddot{\phi} + 3H\dot{\phi} - \frac{\nabla^2 \phi}{a^2} + V'(\phi) = 0, \quad (2.54)$$

where $\dot{V}(\phi) = \frac{dV(\phi)}{d\phi}$ and $3H\dot{\phi}$ represents the friction term. The energy-momentum tensor corresponding to the inflaton is given by:

$$T_{\mu\nu} = \partial_\mu \phi \partial_\nu \phi - g_{\mu\nu} \mathcal{L}. \quad (2.55)$$

The expressions for the energy density ρ_ϕ and the pressure p_ϕ , treated as a perfect fluid, are:

$$T_{00} = \rho_\phi = \frac{1}{2} \dot{\phi}^2 + V(\phi) + \frac{1}{2} \nabla \phi^2. \quad (2.56)$$

$$T_{ii} = p_\phi = \frac{1}{2} \dot{\phi}^2 - V(\phi) - \frac{1}{6} \nabla \phi^2. \quad (2.57)$$

From Eqs. (2.56) and (2.57) we can notice that if the terms with the gradients are dominant over the rest of expressions¹, we obtain:

$$\rho_\phi = \frac{1}{2} \nabla \phi^2, \quad (2.58)$$

$$-3p_\phi = \frac{1}{2} \nabla \phi^2, \quad (2.59)$$

If we equate Eqs. (2.58) and (2.59) we will obtain that $p_\phi = -\rho_\phi/3$ which would not lead us towards a period of inflation¹⁵. On the other hand, if we consider a homogeneous field where $\nabla \phi = 0$, we obtain an equation of state:

$$w = \frac{p_\phi}{\rho_\phi} = \frac{\frac{1}{2} \dot{\phi}^2 - V(\phi)}{\frac{1}{2} \dot{\phi}^2 + V(\phi)}. \quad (2.60)$$

With this in mind, we can separate the inflation field into:

$$\phi(t) = \phi_0(t) + \delta\phi(\mathbf{x}, t). \quad (2.61)$$

where $\phi_0(t)$ is the classical inflaton field on the initial isotropic and homogeneous state, while $\delta\phi(x, t)$ describes the quantum fluctuations $\nabla \phi = 0$ around ϕ_0 ¹¹². The separation made in Eq. (2.61) is done because the value of the

classical inflaton is much larger than the value of the quantum fluctuations. Then, the energy-momentum tensor with this last condition ($\nabla\phi = 0$) is:

$$T_{00} = \rho_\phi = \frac{\dot{\phi}^2}{2} + V(\phi), \quad (2.62)$$

$$T_{ii} = p_\phi = \frac{\dot{\phi}^2}{2} - V(\phi), \quad (2.63)$$

The kinetic energy of field is represented by $\dot{\phi}^2$. If we consider that our potential $V(\phi) \gg \dot{\phi}^2$ the first term of Eqs. (2.62) and (2.63) can be neglected and we obtain the following condition¹³:

$$p_\phi \approx -\rho_\phi. \quad (2.64)$$

From this last result obtained in Eq. (2.64) we can interpret that we have inflation if the potential energy of the scalar field dominates in a large proportion over the kinetic quantity¹⁵.

2.6 Equations of motion

We can obtain the equations of motion if we plug Eq. (2.62) and Eq. (2.63) into the Friedmann equation (2.16) and fluid equations (2.17).

$$H^2 = \frac{1}{3M_{\text{pl}}^2} \left(V(\phi) + \frac{1}{2}\dot{\phi}^2 \right), \quad (2.65)$$

or

$$H^2 = l^2 \left(V(\phi) + \frac{1}{2}\dot{\phi}^2 \right). \quad (2.66)$$

and

$$\ddot{\phi} + 3H\dot{\phi} + V'(\phi) = 0 \quad (2.67)$$

This last system is known as the Klein-Gordon equation, where $V'(\phi) = \partial V/\partial\phi$. In Eq. (2.65) the term that describes the curvature is ignored because the system is not affected by including or ignoring said quantity. This is because that during inflation Λ becomes subdominant¹³. In the inflation period, the condition $V(\phi) > \dot{\phi}^2$ must be fulfilled in a simple way if one has the adequate potential¹. In Eq. (2.67) we can show that the evolution of the scalar field is contained with an second-order ordinary differential equation whose solution will vary depending on the initial conditions that are given to it. The attractor behavior within these different solutions will be of great importance in the different inflationary models, since with this we can ensure that the variations present in the different results are quickly canceled out, and therefore that these models are predictive¹³.

Chapter 3

Methodology

3.1 Slow-Roll Approximation

So far we have seen how the cosmological constant Λ can create an exaggeratedly accelerated period of expansion, which solves the problems left by the Big Bang theory. A short time after inflation has started, it must end and the energy that dominates the Universe turns into matter; This process is known as reheating. In this reheating process, the cosmological constant, which dominates the Universe, breaks down into elementary particles¹¹⁷. One of the characteristics of scalar fields is that they can behave like a dynamic cosmological constant. With this in mind, it is convenient to look for a simple model for the equations of Friedman (2.65) and Klein-Gordon (2.67), where the kinetic energy of the scalar field is much less than its potential energy and the acceleration can be neglected, that is say $V(\phi) \gg \dot{\phi}^2$ and $V'(\phi) \gg \ddot{\phi}$ ¹¹¹³. Then, the equations of motion, with these conditions, for slow-roll inflation becomes:

$$3H\dot{\phi} \simeq -V(\phi), \quad (3.1)$$

$$H^2 \simeq \frac{8\pi}{3M_{pl}^2} V(\phi). \quad (3.2)$$

In Fig. (3.1) we can see how when the kinetic part of the inflaton field is comparable to the potential field, the inflationary process ends up giving rise to overheating¹. For this Slow-roll approach to be valid, two conditions must be satisfied:

$$\epsilon(\phi) \ll 1, \quad (3.3)$$

$$|\eta(\phi)| \ll 1. \quad (3.4)$$

where ϵ and η are the slow-roll parameters whose definitions with respect to the potential $V(\phi)$ are:

$$\epsilon(\phi) = \frac{M_{pl}^2}{2} \left(\frac{V'}{V} \right)^2, \quad (3.5)$$

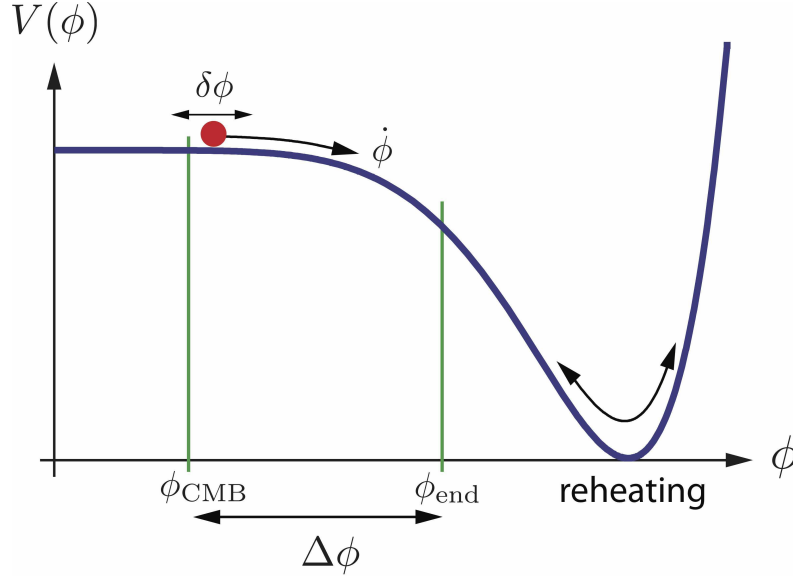


Figure 3.1: Representation of an inflation potential. The accelerated expansion of the Universe occurs when the potential energy of the field, V_ϕ , is vastly greater than its kinetic energy ($\frac{\dot{\phi}^2}{2}$). Inflation ends when $V_\phi \approx \frac{\dot{\phi}^2}{2}$. CMB fluctuations are created by quantum fluctuations, $\delta\phi$, about 60 e-folds before the end of inflation²

$$\eta(\phi) = M_{pl}^2 \frac{V'''}{V}. \quad (3.6)$$

By definition we note that it is positive and its physical meaning can be derived from combining Eqs. (2.65) and (2.67) to obtain \ddot{a} :

$$\frac{\ddot{a}}{a} = H^2(1 - \epsilon). \quad (3.7)$$

Therefore, to fulfill the condition of having an accelerated expansion $\ddot{a} > 0$, from Eqs. (3.3) and (3.4) we will obtain that $\epsilon < 1$. The slow-roll approximations equations (3.1) and (3.2) reduce the equations of motion of the inflation period by one degree, which makes $\dot{\phi}$ stop being a free parameter, as was the case in equation (2.67), so that its value initial depends on the slow-roll equations¹³. Given a potential, the slow-roll parameters make it easier to determine where inflation will occur.

3.1.1 Relation Between Slow-Roll and Inflation

In the previous section we saw how slow-roll conditions and parameters are sufficient requirements for the existence of the inflation period. We can affirm this by rewriting:

$$\frac{\ddot{a}}{a} = \dot{H} + H^2 > 0, \quad (3.8)$$

Since H^2 will always be positive, the condition is satisfied if $H^2 > H$, if H is also positive, or in turn if:

$$-\frac{\dot{H}}{H^2} < 1, \quad (3.9)$$

So we can see how Eq. (3.5), for $\epsilon < 1$, becomes:

$$-\frac{\dot{H}}{H^2} \simeq \frac{M_{pl}^2}{2} \left(\frac{V'}{V} \right)^2 = \epsilon. \quad (3.10)$$

Since inflation can continue even when slow-roll conditions are violated, these impositions turn out to be sufficient but not necessary. If it is desired to put an end to the inflation period in the cosmological models, these conditions must be broken in such a way that their potential energy tends to zero or its quantity can be insignificant¹¹.

3.2 Cosmological Perturbations in the Geometry of the Universe

As has been seen so far, the Universe in its early beginnings was extremely homogeneous and isotropic, so it was necessary to introduce small perturbations to explain the construction of the large-scale structure of the Universe, from the inhomogeneities created by these primordial disturbances. Currently these inhomogeneities are evident on small scales and will grow due to the attractive force of gravity^{18 19}.

Most evolution of the inhomogeneities can be treated as linear disturbances, which are no longer valid in the recent past. That said, we can write a new system that includes such disturbances, $\delta g_{\mu\nu}$, and the FLRW background metric $g_{\mu\nu}$.

$$\bar{g}_{\mu\nu} = \delta g_{\mu\nu} + g_{\mu\nu}. \quad (3.11)$$

Equation (3.11) must satisfy the condition $\delta g_{\mu\nu} < g_{\mu\nu}$ obviously.

The cosmological models of inflation, applied within General Relativity, are of great importance for the approach of the theory of perturbations. These inflationary models generate density perturbations, also known as scalar perturbations, or gravitational waves. Scalar and tensor perturbations evolve independently, so they can be analyzed autonomously. The increasing inhomogeneities that give rise to the large-scale structure of the Universe and the anisotropies observed in the CMB, have scalar perturbations in the leading role, due to the fact that they present instabilities. On the other hand, for the stability within the tensor disturbances, these could not contribute to the formation of matter, but they represent a small percentage of anisotropies in the CMB^{13 20}.

Dodelson²¹ was one of the people who studied the perturbed Einstein tensor:

$$\delta G_{\nu}^{\mu} = 8\pi G \delta T_{\nu}^{\mu}, \quad (3.12)$$

where $T_{\mu\nu}$ corresponds to the perturbed energy-momentum tensor. If we add the unperturbed linearized Einstein tensor to Eq. (3.12), we will obtain:

$$G_{\mu\nu}^{(0)} + \delta G_{\mu\nu} = 8\pi G [T_{\mu\nu}^{(0)} + \delta T_{\mu\nu}], \quad (3.13)$$

We can represent the FLRW metric with respect to linear perturbations as follows:

$$ds^2 = a^2 [-(1 + 2A)d\eta^2 + 2B_i dx^i d\eta + (\delta_{ij} + h_{ij})dx^i dx^j], \quad (3.14)$$

where B_i and S_{ij} represent the vector and the spatial metric, respectively. Furthermore, A appears as a scalar and h_{ij} takes the name of symmetric tensor, whose matrix is:

$$h_{ij} = a^2 \begin{pmatrix} 1 + h_+ & h_\times & 0 \\ h_\times & 1 - h_+ & 0 \\ 0 & 0 & 1 \end{pmatrix}, \quad (3.15)$$

where h_+ and h_\times are two functions whose quantities are small. Furthermore, the spatial elements can be represented by the disturbance tensor as:

$$\mathcal{H}_{ij} = \begin{pmatrix} h_+ & h_\times & 0 \\ h_\times & -h_+ & 0 \\ 0 & 0 & 0 \end{pmatrix}. \quad (3.16)$$

In the same way as in Eq. (3.15), h_+ and h_\times are two components of a divergenless, traceless, and symmetric tensor in which $k^{i,j}H_{ij} = 0$. From this, we can start by calculating the Cristoffel symbols:

$$\begin{aligned} \Gamma_{\alpha\beta}^\mu &= \frac{1}{2}g^{\mu\nu} (g_{\mu\nu,\beta} + g_{\mu\nu,\alpha} - g_{\alpha\beta,\mu}), \\ \Gamma_{00}^0 &= 0, \\ \Gamma_{i0}^0 &= \Gamma_{0i}^0 = 0, \\ \Gamma_{00}^i &= 0, \\ \Gamma_{ij}^0 &= Hg_{ij} + \frac{a^2\mathcal{H}_{ij,0}}{2}, \\ \Gamma_{0j}^i &= \Gamma_{j0}^i = H\delta_{ij} + \frac{1}{2}\mathcal{H}_{ij,0}, \\ \Gamma_{jk}^i &= \frac{i}{2} [k_k\mathcal{H}_{ij} + k_j\mathcal{H}_{ik} + k_i\mathcal{H}_{jk}]. \end{aligned} \quad (3.17)$$

Once these calculations have been made, we can find the Ricci tensor and then its scalar:

$$\begin{aligned} R_{\mu\nu} &= \Gamma_{\mu\nu,\alpha}^\alpha - \Gamma_{\mu\alpha,\nu}^\alpha + \Gamma_{\beta\alpha}^\alpha \Gamma_{\mu\nu}^\beta - \Gamma_{\beta\nu}^\alpha \Gamma_{\mu\alpha}^\beta, \\ R_{00} &= -3\frac{\ddot{a}}{a}, \\ R_{0i} &= 0, \\ R_{ij} &= g_{ij} \left(\frac{\ddot{a}}{a} + 2H^2 \right) + \frac{3}{2}a^2 H \mathcal{H}_{ij,0} + a^2 \frac{\mathcal{H}_{ij,00}}{2} + \frac{k^2}{2} \mathcal{H}_{ij}. \end{aligned} \quad (3.18)$$

with the Ricci scalar:

$$\mathcal{R} = g^{00}R_{00} + g^{ij}R_{ij}, \quad (3.19)$$

which give us:

$$\mathcal{R} = 0. \quad (3.20)$$

The value obtained for \mathcal{R} expresses the little relevance that perturbations have in the Ricci scalar. All this process carried out helps us to find the Einstein tensor:

$$G_\nu^\mu = R_\nu^\mu - \frac{1}{2}g_\nu^\mu \mathcal{R}, \quad (3.21)$$

Considering the value of the Ricci scalar Eq. (3.20), within the Eq. (3.21), we obtain that:

$$\begin{aligned} \delta G_0^0 &= 0, \\ \delta G_0^i &= 0, \\ \delta G_j^i &= \delta^{ik} \left[\frac{3}{2} H \mathcal{H}_{kj,0} + \frac{\mathcal{H}_{kj,00}}{2} + \frac{k^2}{2a^2} \mathcal{H}_{kj} \right]. \end{aligned} \quad (3.22)$$

It is important to mention that the conformal time (η) can be written in terms of the comoving time (t) as follows:

$$\eta = \int \frac{dt}{a(t)}. \quad (3.23)$$

3.2.1 Quantum Perturbations

As we have seen previously, during the inflation period the early Universe was governed by the components of a uniform scalar field and an uniform background metric. For this reason, it is convenient to work with the quantum perturbations of the field against the background, in the same way as was done with the classical equations of motion in general relativity²¹.

From Einstein's perturbed equation, we can obtain the equations of motion for the perturbations. For this, we must replace the time-time, time-space and space-space components in the perturbed Einstein equation obtained in Eq. (3.24), which will only result in space-space components, so we can analyze how the quantities h_+ and h_x evolve.

Let us analyze the h_+ component, remembering the proportionality that \mathcal{H}_{ij} presents in equation (3.24), where $\mathcal{H}_{11} = h_x = -\mathcal{H}_{22}$. Realizing a spatial difference between δG_1^1 and δG_2^2 , we obtain the solution:

$$\delta G_1^1 - \delta G_2^2 = 3Hh_{+,0} + h_{+,00} + \frac{k^2 h_+}{a^2}. \quad (3.24)$$

As we already know, we only have space-space components, that is, we have $\delta G_j^i = 0$. Considering this situation, we can rewrite Eq. (3.24) as:

$$3Hh_{+,0} + h_{+,00} + \frac{k^2 h_+}{a^2} = 0, \quad (3.25)$$

Doing the same analysis for h_x and expressing it in a general way together with h_+ , we will obtain an equation with the shape of a wave:

$$\ddot{h}_{+,x} + 3H\dot{h}_{+,x} + \frac{k^2}{a^2} h_{+,x} = 0, \quad (3.26)$$

Furthermore, we can represent this function in terms of the conformal time, so we make the change $\dot{h}_{+,x} = h'_{+,x}/a$ to which will give us:

$$h''_{+,x} + 2\mathcal{H}h'_{+,x} + k^2 h_{+,x} = 0. \quad (3.27)$$

The last Eqs. (3.26) and (3.27) are known as gravity waves. With all the analysis carried out so far to find a solution to Eq. (3.27), we proceed to quantify said function, thereby defining a possible solution with the structure of a harmonic oscillator:

$$\tilde{h} \equiv \frac{ah}{\sqrt{16\pi G}}. \quad (3.28)$$

In Eq. (3.28) we can see a possible solution, to check this we can analyze this equation with respect to h , that is, we need to clear this quantity and derive it twice with respect to η ,

$$h' = \sqrt{16\pi G} \left(\frac{\tilde{h}'}{a} - \frac{a'}{a^2} \tilde{h} \right), \quad (3.29)$$

$$h'' = \sqrt{16\pi G} \left(\frac{\tilde{h}''}{a} - 2 \frac{a'}{a^2} \tilde{h}' - \frac{a''}{a^2} \tilde{h} + 2 \frac{(a')^2}{a^3} \tilde{h} \right). \quad (3.30)$$

Replacing these last expressions in Eq. (3.28) and separating the common factor $\sqrt{16\pi G}$:

$$\sqrt{16\pi G} \left[\left(\frac{\tilde{h}''}{a} - 2 \frac{a'}{a^2} \tilde{h}' - \frac{a''}{a^2} \tilde{h} + 2 \frac{(a')^2}{a^3} \tilde{h} \right) + 2 \frac{a'}{a} \left(\frac{\tilde{h}'}{a} - \frac{a'}{a^2} \tilde{h} \right) + k^2 \left(\frac{h'}{a} \right) \right] = 0. \quad (3.31)$$

In order to simplify this equation, we divide the last equation by its common factor and suppress the repeated quantities with opposite sign, we have:

$$\frac{1}{a} \left[\tilde{h}'' + \left(k^2 - \frac{a''}{a} \right) \tilde{h} \right] = 0, \quad (3.32)$$

It can be seen that Eq. (3.32) keeps the structure of a harmonic oscillator, which implies that h acts as a quantum operator whose expression would be given by:

$$\hat{h}(\vec{k}, \eta) = v(k, \eta) \hat{a}_{\vec{k}} + v^*(k, \eta) a_{\vec{k}}^\dagger, \quad (3.33)$$

where $a_{\vec{k}}^\dagger$ and $\hat{a}_{\vec{k}}$ are the coefficient of creation and destruction respectively, which satisfy the equation for gravitational waves:

$$v_k'' + \left(k^2 - \frac{a''}{a} \right) v_k = 0. \quad (3.34)$$

In the last expression $v_k = a\psi_k$, been ψ the representation of tensor perturbations. In slow-roll inflation $a''/a \approx 2a^2H^2$ and the behavior of v_k is characterized by whether the mode is inside or outside the horizon²²:

$$v_k \rightarrow \frac{1}{\sqrt{2k}} e^{-ik\tau} \quad \text{as} \quad aH/k \rightarrow 0, \quad (3.35)$$

$$v_k \propto a \quad \text{for} \quad aH/k \gg 1. \quad (3.36)$$

Equation (3.34) is a second order ODE, so it is convenient to use a slow-roll approach in order to reduce its degree of difficulty and find a solution to the equality. Considering the transformation $a' = -a/\eta$, we can find the Mukhanov-Sasaki equation:

$$v_k'' + \left(k^2 - \frac{2}{\eta^2} \right) v_k = 0. \quad (3.37)$$

3.2.2 Scalar perturbations equation

The detailed calculations of the results that will be shown in this section, were calculated by Tapia¹⁸ in his article "Scalar Cosmological Perturbations".

As in the previous section, let us start by rewriting the FLRW perturbed metric, but this time in terms of the gauge invariant variables Φ and Ψ .

$$ds^2 = -[1 + 2\Phi(t, x)]dt^2 + a^2[1 - 2\Psi(t, x)]\delta_{ij} dx^i dx^j, \quad (3.38)$$

The covariant $g_{\mu\nu}$ and contravariant $g^{\mu\nu}$ matrices considered in metric (3.38) are given by:

$$g_{\mu\nu} = \begin{pmatrix} -1 - 2\Phi(t, x) & 0 & 0 & 0 \\ 0 & a^2[1 - 2\Psi(t, x)] & 0 & 0 \\ 0 & 0 & a^2[1 - 2\Psi(t, x)] & 0 \\ 0 & 0 & 0 & a^2[1 - 2\Psi(t, x)] \end{pmatrix}, \quad (3.39)$$

and

$$g^{\mu\nu} = \begin{pmatrix} -\frac{1}{1+2\Phi(t,x)} & 0 & 0 & 0 \\ 0 & \frac{1}{a^2[1-2\Psi(t,x)]} & 0 & 0 \\ 0 & 0 & \frac{1}{a^2[1-2\Psi(t,x)]} & 0 \\ 0 & 0 & 0 & \frac{1}{a^2[1-2\Psi(t,x)]} \end{pmatrix}. \quad (3.40)$$

In the same way, let's start calculating the Christoffel symbols keeping the terms up to first order:

$$\begin{aligned} \Gamma_{00}^0 &= \frac{1}{2}(-1 + 2\Phi)(-2\Phi_{,0}), \\ \Gamma_{0i}^0 &= \frac{1}{2}(-1 + 2\Phi)(-2\Phi_{,i}), \\ \Gamma_{ij}^0 &= -\frac{1}{2}\delta_{ij}(-1 + 2\Phi)[a^2(1 - 2\Psi)]_{,0}, \\ \Gamma_{00}^i &= \frac{1}{2}\delta_{ij}a^{-2}(1 + 2\Psi)(2\Phi_{,i}), \\ \Gamma_{j0}^i &= \frac{1}{2}\delta_{ij}a^{-2}(1 + 2\Psi)[a^2(1 - 2\Psi)]_{,0}, \\ \Gamma_{jk}^i &= \frac{1}{2}a^{-2}(1 + 2\Psi)[\delta_{ij}a^2(1 - 2\Psi)_{,k} + \delta_{ik}a^2(1 - 2\Psi)_{,j} - \delta_{jk}a^2(1 - 2\Psi)_{,i}], \\ &= (1 + 2\Psi)(-\delta_{ij}\Psi_{,k} - \delta_{ik}\Psi_{,j} + \delta_{jk}\Psi_{,i}). \end{aligned} \quad (3.41)$$

Now, we can find the Ricci tensor for time-time, time-space, and space-space components:

$$\begin{aligned}
R_{00} &= a^{-2}\Phi_{,ii} - 3\left(\frac{\ddot{a}}{a} - H^2 - \Psi_{,00}\right) + 3H\Phi_{,0} - 3(H^2 - 2H\Psi_{,0}), \\
\delta R_{00} &= a^{-2}\left[\nabla^2\Phi + 3\Psi'' + 3\mathcal{H}(\Phi' + \Psi')\right], \\
R_{0i} &= \dot{\Phi}_{,i} - \dot{\Phi}_{,i} + \delta_{ij}(H - \dot{\Psi})_{,i} - \delta_{ij}(H - \dot{\Psi})_{,i} + \delta_{ij}(H - \dot{\Psi})\Phi_{,i}, \\
&\quad - \delta_{ij}(H - \dot{\Psi})\Phi_{,j} + \delta_{ik}\Phi_{,k}(H - \dot{\Psi}) - \delta_{ki}[H - 2H(\Phi + \Psi) - \dot{\Psi}]\Phi_{,k}, \\
&\quad + (-\delta_{jk}\Psi_{,j} - \delta_{ij}\Psi_{,i} + \delta_{ij}\Psi_{,j})(H - \dot{\Psi}) - (-\delta_{kk}\Psi_{,i} - \delta_{ki}\Psi_{,k} + \delta_{ki}\Psi_{,k})(H - \dot{\Psi}), \\
\delta R_{0i} &= \frac{2}{a}(\Psi'_{,i} + \mathcal{H}\Phi_{,i}), \\
R_{ij} &= \delta_{ij}\left\{\nabla^2\Psi - \Psi'' + [1 - 2(\Phi + \Psi)](\mathcal{H}' + 2\mathcal{H}^2) - \mathcal{H}(\Phi' + 5\Psi')\right\} - (\Phi - \Psi)_{,ij}.
\end{aligned} \tag{3.42}$$

and the first-order Ricci scalar:

$$\mathcal{R} = -\frac{2}{a^2}\left[3\Psi'' + \nabla^2(\Phi - 2\Psi) + 3\mathcal{H}(\Phi' + 3\Psi') - 3(\mathcal{H}' + \mathcal{H}^2) + 6\Phi(\mathcal{H}' + \mathcal{H}^2)\right]. \tag{3.43}$$

The components presented in the Ricci tensor are:

$$\mathcal{H} = \frac{a'}{a}; \quad H = \frac{\mathcal{H}}{a}. \tag{3.44}$$

As before we can calculate the time-time, time-space, and space-space components for the Einstein tensor:

$$\begin{aligned}
G_{00} &= \frac{1}{a^2}\left[-6\mathcal{H}\Psi' + 2\nabla^2\Psi + 3\mathcal{H}^2\right], \\
G_{0i} &= 2a^{-1}(\Psi'_{,i} + \mathcal{H}\Phi_{,i}), \\
&= \delta R_{0i}. \\
G_{ij} &= \delta_{ij}\left[-(2\mathcal{H}' + \mathcal{H}^2) + 2\Psi'' + \nabla^2(\Phi - \Psi) + 2(2\mathcal{H}' + \mathcal{H}^2)(\Psi + \Phi) + 2\mathcal{H}(\Phi' + 2\Psi')\right] \\
&\quad + (\Psi - \Phi)_{,ij}.
\end{aligned} \tag{3.45}$$

Converting tensors G_{00} , G_{0i} , G_{ij} to mixed tensors and linearizing them with respect to the background. For the time-time component:

$$\begin{aligned}
G_0^0 &= g^{\mu 0}G_{\mu 0} = g^{00}G_{00}, \\
&= (-1 + 2\Phi)a^{-2}\left[-6\mathcal{H}\Psi' + 2\nabla^2\Psi + 3\mathcal{H}^2\right], \\
&= a^{-2}\left[-3\mathcal{H}^2 + 6\mathcal{H}\Psi' - 2\nabla^2\Psi + 6\mathcal{H}^2\Phi\right], \\
\delta G_0^0 &= a^{-2}\left[6\mathcal{H}\Psi' - 2\nabla^2\Psi + 6\mathcal{H}^2\Phi\right].
\end{aligned} \tag{3.46}$$

In the time-space component, the tensor is perturbation, then:

$$\begin{aligned}
\delta G_i^0 &= g^{\mu 0}G_{\mu i}, \\
&= g^{00}G_{0i}, \\
&= (-1 + 2\Phi)2a^{-1}(\Psi'_{,i} + \mathcal{H}\Phi_{,i}), \\
&= -2a^{-1}(\Psi' + \mathcal{H}\Phi)_{,i}.
\end{aligned} \tag{3.47}$$

and the space-space component:

$$\begin{aligned}
G_j^i &= g^{\mu i} G_{\mu j}, \\
&= a^{-2} (1 + 2\Psi) \left\{ \delta_{ij} \left[- (2\mathcal{H}' + \mathcal{H}^2) + 2\Psi'' + \nabla^2 (\Phi - \Psi) + 2 (2\mathcal{H}' + \mathcal{H}^2) (\Psi + \Phi) \right. \right. \\
&\quad \left. \left. + 2\mathcal{H} (\Phi' + 2\Psi') \right] + (\Psi - \Phi)_{,ij} \right\}, \\
&= a^{-2} \left\{ \delta_{ij} \left[- (2\mathcal{H}' + \mathcal{H}^2) + \nabla^2 (\Phi - \Psi) + 2\Psi'' + 2 (2\mathcal{H}' + \mathcal{H}^2) \Phi + 2\mathcal{H} (\Phi' + 2\Psi') \right] \right. \\
&\quad \left. + (\Psi - \Phi)_{,ij} \right\}, \\
\delta G_j^i &= a^{-2} \left\{ \delta_{ij} \left[\nabla^2 (\Phi - \Psi) + 2\Psi'' + 2 (2\mathcal{H}' + \mathcal{H}^2) \Phi + 2\mathcal{H} (\Phi' + 2\Psi') \right] + (\Psi - \Phi)_{,ij} \right\}.
\end{aligned} \tag{3.48}$$

For the energy-momentum tensor, we can rewrite the definition given in Eq. (2.55).

$$T_\nu^\mu = \partial^\mu \phi \partial_\nu \phi - \left[\frac{1}{2} \partial^\alpha \phi \partial_\alpha \phi + V \right] \delta_\nu^\mu. \tag{3.49}$$

If a linear perturbation is added to the inflaton field, we obtain:

$$\phi(t, \mathbf{x}) = \phi_0(t) + \delta\phi(t, \mathbf{x}). \tag{3.50}$$

The quantities ϕ_0 and $\delta\phi$ represent the background field and the linear perturbation, respectively. As with the $g_{\nu\mu}$ metric, this perturbed field must satisfy the condition $\phi_0 \geq \delta\phi$. Calculating the time-time, time-space, and space-space components:

$$\begin{aligned}
T_0^0 &= a^{-2} \left[-\frac{\phi'^2}{2} - a^2 V(\phi_0) + \Phi \phi_0'^2 - \phi_0' \delta\phi' - a^2 \delta\phi V_{,\phi} \right], \\
T_i^0 &= -a^{-1} \phi_0' \delta\phi_{,i}, \\
&= \delta T_i^0, \\
T_j^i &= \delta_{ij} a^{-2} \left[\frac{(\phi_0')^2}{2} - a^2 V(\phi_0) - \Phi (\phi_0')^2 + \phi_0' \delta\phi' - a^2 \delta\phi V_{,\phi} \right].
\end{aligned} \tag{3.51}$$

Once again, linearizing T_0^0 , T_i^0 and T_j^i with respect to the background:

$$\begin{aligned}
\delta T_0^0 &= a^{-2} (\Phi \phi_0'^2 - \phi_0' \delta\phi' - a^2 \delta\phi V_{,\phi}), \\
\delta T_i^0 &= T_i^0, \\
\delta T_j^i &= \frac{\delta_{ij}}{a^2} \left[-\Phi (\phi_0')^2 + \phi_0' \delta\phi' - a^2 \delta\phi V_{,\phi} \right].
\end{aligned} \tag{3.52}$$

If we compare the linearized equations of the space-space components of the energy-momentum tensor (3.52) and Einstein tensor (3.48), we can notice that $\Phi = \Psi$ when $i \neq j$. We just have 3 resulting equations:

$$\nabla^2 \Phi - 3\mathcal{H}\Phi' - (\mathcal{H}' + 2\mathcal{H}^2)\Phi = \frac{3}{2} l^2 (\phi_0' \delta\phi' + V_{,\phi} a^2 \delta\phi). \tag{3.53}$$

$$\Phi' + \mathcal{H}\Phi = \frac{3}{2}l^2\phi'_0\delta\phi, \quad (3.54)$$

$$\Phi'' + 3\mathcal{H}\Phi' + (\mathcal{H}' + 2\mathcal{H}^2)\Phi = \frac{3}{2}l^2(\phi'_0\delta\phi' - V_{,\phi}\alpha^2\delta\phi). \quad (3.55)$$

Equation (2.66) can be rewritten with respect to conformal time as follows:

$$\frac{V_{,\phi_0}}{\phi'_0} = -\frac{1}{a^2} \left[\frac{\phi''_0}{\phi'_0} + 2\mathcal{H} \right]. \quad (3.56)$$

If we subtract equations (3.53) and (3.55) and plug $\delta\phi$ into equation (3.54) we get a single second order differential equation:

$$\Phi'' - \nabla^2\Phi + \Phi \left[2\mathcal{H} - 2\frac{\phi''_0}{\phi'_0} \right] + \Phi \left[2\mathcal{H}' - \frac{2\mathcal{H}\phi''_0}{\phi'_0} \right] = 0. \quad (3.57)$$

Taking the changes of variable $u = (a/\phi'_0)\Phi$ and $z = (a\phi'_0)/\mathcal{H}$ the Eq. (3.57) takes the form:

$$u'' - \nabla^2u - z \left(\frac{1}{z} \right)'' u = 0. \quad (3.58)$$

To study the perturbation inside the horizon, we can use Eq. (3.58) to arrive at the equation that describes these perturbations¹⁸. To find these perturbation equations, Deruelle²³ considers the gauge invariant variable:

$$v = a \left[\delta\phi + \frac{\phi_0\Phi}{\mathcal{H}} \right]. \quad (3.59)$$

The equation (3.59) can be described in terms of u by:

$$v = \frac{2}{3l^2} \left(u' + \frac{z'}{z}u \right), \quad (3.60)$$

Differentiating twice this last expression with respect to conformal time, it can be replaced in ODE (3.58) to satisfy that equation. So we get:

$$\nabla^2u = \frac{3}{2}l^2z \left(\frac{v}{z} \right)', \quad (3.61)$$

Multiplying the expression ∇^2 in Eq. (3.58):

$$\nabla^2(u)'' - \nabla^2(\nabla^2u) - z \left(\frac{1}{z} \right)'' \nabla^2u = 0, \quad (3.62)$$

This allows us to replace Eq. (3.61) in Eq. (3.62):

$$\left[\left(v' - \frac{z'}{z}v \right) \right]'' - \nabla^2 \left[z \left(\frac{v}{z} \right)' \right] - \left(\frac{2z'}{z^2} - \frac{z''}{z} \right) \left(v' - \frac{z'}{z}v \right) = 0, \quad (3.63)$$

From this last equality we obtain the solution:

$$z \left(\frac{v'' - \nabla^2v - \frac{z''}{z}v}{z} \right)' = 0, \quad (3.64)$$

Finally, the equation of motion in the Fourier space is obtained:

$$u_k'' + \left(k^2 - \frac{z''}{z} \right) u_k = 0. \quad (3.65)$$

Considering the limit $k^2 \gg z''/z$, the factor u_k tends to:

$$u_k \rightarrow \frac{1}{\sqrt{2k}} e^{-ik\tau}. \quad (3.66)$$

3.2.3 Power Spectrum for Perturbations

The power spectrum is a tool that helps to statistically characterize the properties of fluctuations in inflation models, and is defined by:

$$P_\chi(k) = \frac{k^3}{2\pi^2} |\chi_k|, \quad (3.67)$$

where χ_k represents a random quantity of the power spectrum $P_\chi(k)$. If we want to represent this last expression as a power function, we will obtain:

$$P_\chi(k) = A(k) \left(\frac{k}{k_0} \right)^{n_\chi - 1}, \quad (3.68)$$

where k represents a chosen pivot that is usually represented by k_0 . The function n_χ that fulfills the spectral index function in Eq. (3.68) is defined as:

$$n_\chi - 1 = \frac{\ln P_\chi}{d \ln k}, \quad (3.69)$$

The function on the right, dependent on the logarithm, can be expanded as follows:

$$\frac{\ln P_\chi}{d \ln k} = \left(\frac{d \ln P_\chi}{dt} \right) \left(\frac{dt}{d \ln a} \right) \left(\frac{d \ln a}{d \ln k} \right). \quad (3.70)$$

3.2.4 The Power law case

When the tensor perturbations are taken into account, we can use equation (3.68) to write scalar and tensor power spectra³ as:

$$\mathcal{P}_S(k) = A_S \left(\frac{k}{k_0} \right)^{n_S - 1}, \quad (3.71)$$

and

$$\mathcal{P}_T(k) = A_T \left(\frac{k}{k_0} \right)^{n_T}, \quad (3.72)$$

where A_S , n_S and A_T , n_T represents the amplitude and the spectral indices of the scalar and tensor power spectra. From Eqs. (3.71) and (3.72) we can define the tensor-to-scalar ratio:

$$r(k) = \frac{\mathcal{P}_T(k)}{\mathcal{P}_S(k)}. \quad (3.73)$$

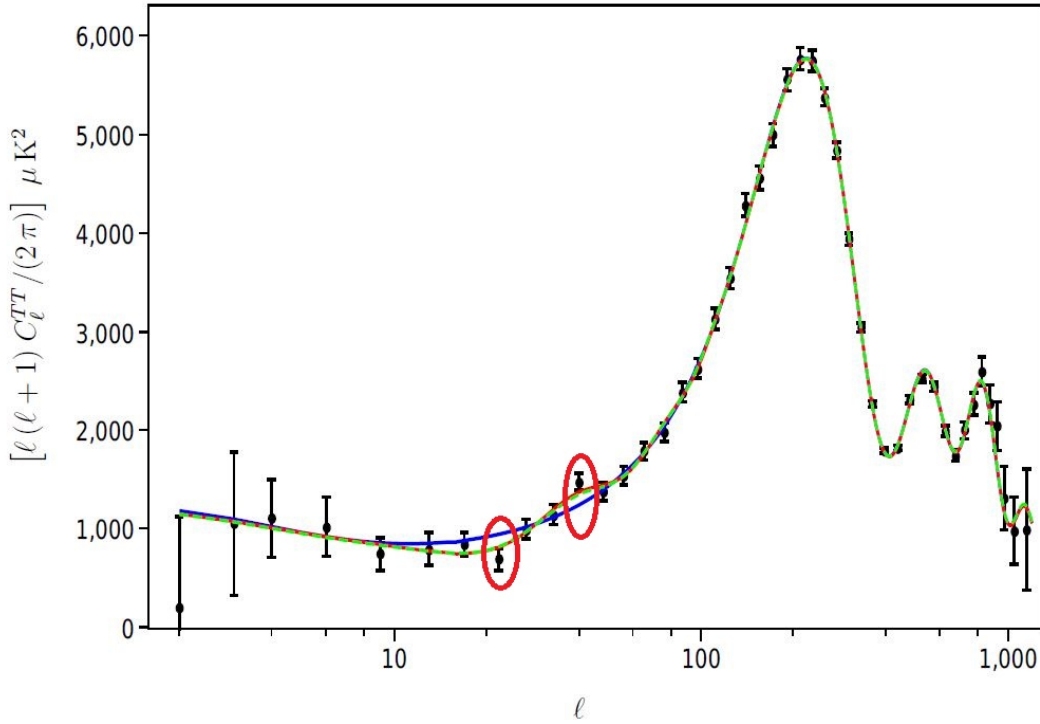


Figure 3.2: The CMB angular power spectrum corresponding to the best fit values of the inflationary models for the WMAP seven-year. The dark dots with its respective error represent the data obtained by WMAP seven-year. The blue line and the dashed green line corresponds corresponds to the chaotic potential without and with a step data³. The red ellipses show the fit that occurs near the multipolar moments $l = 22$ and $l = 40$, due to the step in the chaotic potential.

3.3 Cosmological Inflation Models

Inflation models are of great importance to solve the problems of the initial conditions of the standard cosmological model that describe the evolution of the Universe from the first second to what we currently observe¹¹. Several models have been proposed that satisfactorily do this, among these we can highlight the Starobinsky, small field, tachyon, and chaotic models, among others. These last 3 present certain deficiencies when describing the characteristics of the CMB, as the scalar power spectrum and the angular power spectrum measured by telescopes. Faced with this drawback, the need arises to introduce a small step, in a particular location that generates a burst of oscillations. The presence of oscillations in the scalar power spectrum with particular values in the dimensionless parameters c , d and ϕ_{step} of the chaotic inflationary model with a step, seems to provide a better fit to the angular power spectrum near the multipolar moments $l = 22$ and $l = 40$ ³, as we can see in the Fig. (3.2). This fit helps this inflationary model to show a better approximation with respect to the observational data.

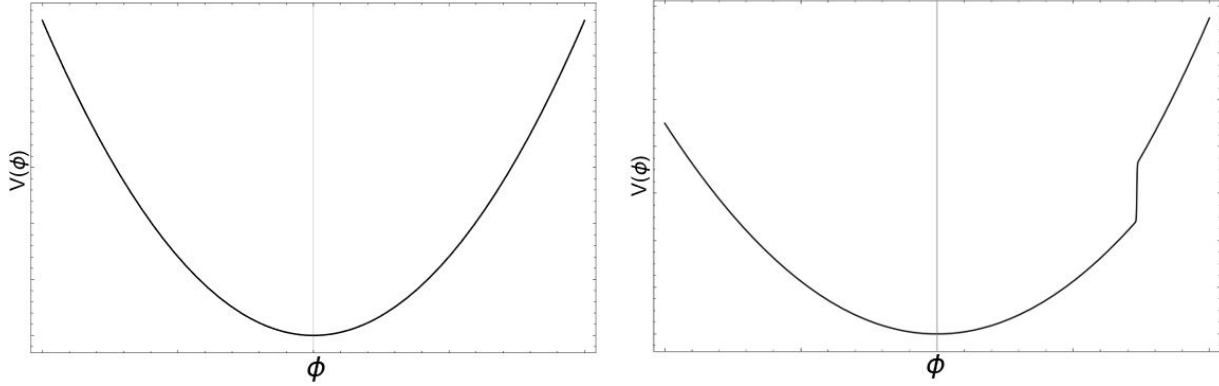


Figure 3.3: The scalar field potential for the chaotic model for $m = 7.5 \times 10^{-6} M_{pl}$. **Left:** without a step. **Right:** with a step with $c = 0.200$, $d = 0.0311$ and $\phi_{step} = 14.670$.

3.3.1 Chaotic Inflationary Model with a Step

For this work we use the chaotic model which is described by the potential:

$$V(\phi) = \frac{1}{2} m^2 \phi^2, \quad (3.74)$$

where m represents the mass of the inflaton. As mentioned above, this is one of the potentials that does not couple correctly to the observations of the CMB, so it is necessary to introduce a small additional step that generates the observed oscillations.

$$V_{step}(\phi) = \left[1 + c \tanh\left(\frac{\phi - \phi_{step}}{d}\right) \right], \quad (3.75)$$

Evidently, c denotes the height of the step, ϕ_{step} its location in the spectrum, and d its inclination³. If we multiply Eqs. (3.74) and (3.75) we will obtain the potential with a step:

$$V(\phi) = \frac{1}{2} m^2 \phi^2 \left[1 + c \tanh\left(\frac{\phi - \phi_{step}}{d}\right) \right]. \quad (3.76)$$

The potential with a step is the one that we are going to use for the numerical analysis and from which we will determine the contribution that Eq. (3.75) adds to Eq. (3.74) to improve the similarity to observational data.

The potential shown on the left side of Fig. (3.3) is also known as the quadratic potential because its behavior closely resembles that obtained with squared powers. On the right side of the same graph, a small jump is shown that occurs due to the introduction of the step in the potential. It is this small jump that produces oscillations in the scalar power spectrum that will be shown in the results section.

Chapter 4

Results and Discussion

4.1 Numerical Analysis of the Chaotic Potential without a step

For the numerical analysis of the chaotic potential with and without a step, the Mathematica code shown in Appendix A was used. According to the observational data, for an inflationary model to be considered partially valid, one of the conditions it must meet is that the final value that its scalar power spectrum follows should be about 2.2×10^{-9} . To compute the values for the power law case, we use $k = 0.002$ and all values taken from the mass of the inflaton m will be in units of M_{pl} .

Let us start this numerical analysis by examining the shape of the chaotic potential without the step for two different values of the mass of the inflaton field (m), as can be seen in Fig. (4.1). For the generation of these graphs, the parameters shown in Table (4.1) were used.

In Fig. (4.1) it can be seen how the final value that the chaotic model takes for $m = 7.5 \times 10^{-6} M_{pl}$ (blue graph), has a good approximation towards a final value of 2.2×10^{-9} (red line) while the graph of the chaotic potential for $m = 6.5 \times 10^{-6} M_{pl}$ (green graph) has a bad approximation to the value that it needs to be considered as a

Model	Parameter	Blue Graph	Green Graph
Chaotic Model without a step	m	7.5×10^{-6}	6.5×10^{-6}
	ϕ_0	15.45000	15.45000
	c	0.00000	0.00000
	ϕ_{step}	0.00000	0.00000
	d	0.00000	0.00000
Power law case	n_s	0.95819	0.96093
	r	0.14216	0.14163

Table 4.1: Parameters used for the graphic representation of Fig. (4.1). The cosmological values n_s and r are obtained for this case.

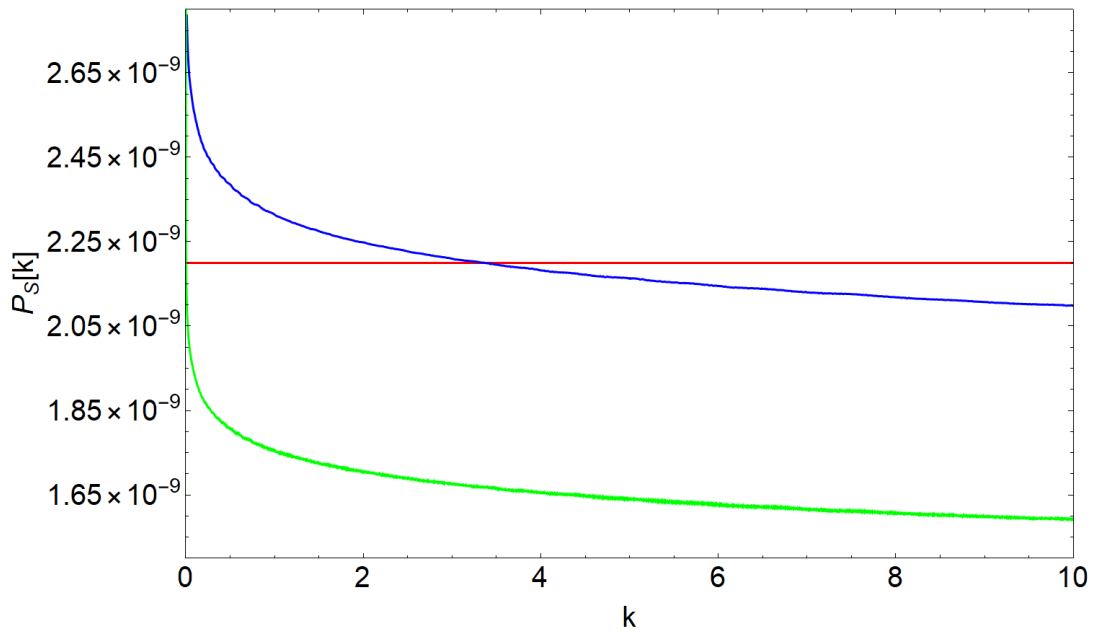


Figure 4.1: Scalar power spectrum for the chaotic potential without the step. The red horizontal line represents the approximate value that the potential must approach for it to be considered a valid model. The parameters used for both the blue color potential and the green color potential are exactly the same except for the value of m ; see Table (4.1). The difference presented by $m = 6.5 \times 10^{-6} M_{pl}$ and $m = 7.5 \times 10^{-6} M_{pl}$ seems to result in a vertical displacement of the potential.

Models	Parameter	Lower limit	Upper limit
Power law case	n_s	0.500	1.500
	r	0.000	1.000
Chaotic model with a step	c	1.3×10^{-2}	1.7×10^{-2}
	ϕ_{step}	13.000	15.000
	d	0.010	0.040

Table 4.2: Range of values that can be considered for the different parameters present in the power law case and the chaotic potential. These limits taken from Dhiraj's³ article were modified considering that there are more combinations of values that the variables of the chaotic potential with a step can have.

good potential. However, the latest observations made by the Planck telescopes, in 2018²⁴, and the WMAP-9 in its ninth year of operation²⁵ record different values in the cosmological parameters, of those calculated numerically, so analytically this model can be neglected. Hence, the idea of introducing a small step in the field of the inflaton that generates oscillations as this helps the values obtained numerically to more accurately resemble those observed by space telescopes.

4.2 Numerical Analysis of the Chaotic Potential with a step

An important point to consider for the analysis of the potential with one step is that the parameters of this potential, specifically ϕ_{step} , c and d , cannot be negative numbers nor can they take excessively high values. Dhiraj et al.,³ in their paper, perform Markov chain Monte-Carlo sampling of the parameter space. This method was used to obtain the parameter constraints in the equations of the chaotic potential and power law case with one step. During the elaboration of this work, the values of the limits considered by Dhiraj were modified, expanding the range of possible values that the parameters of the potential step can take, as shown in the Table (4.2). This new limit table was obtained through a large number of numerical evaluations performed on the chaotic potential with a step where the presence of oscillations in the scalar power spectrum was considered as an acceptance criterion.

These constraints provide a range of values that the parameters that make up the step potential can take, for which the behavior of the scalar spectrum shows oscillations and an approximate final value of 2.2×10^{-9} . The subsequent section shows the numerical analysis performed with different values for c , ϕ_{step} and d that are outside of the established range, to see the importance to considered values inside the limits showed in Table (4.2)

4.2.1 Numerical analysis of the chaotic potential with values outside the limits

Previously, the behavior of the chaotic potential without the step potential was analyzed. In this section we review the trend followed by the graphs for values that are above and below the limits of Table (4.2). If we compare the blue plot in Fig. (4.1) with those obtained in this section, we notice how they are close to being identical, that is, this combination of chosen values is still a poor approximation to the observational data. It is important to clarify

Model	Parameter	Blue Graph (Above the limit)	Purple Graph (Below the limit)
Chaotic Model with a step	$m[M_{pl}]$	7.5×10^{-6}	7.5×10^{-6}
	ϕ_0	15.4500	15.4500
	c	0.01900	0.00120
	ϕ_{step}	17.0000	12.0000
	d	0.07000	0.00900
Power law case	n_s	0.95792	0.95859
	r	0.14124	0.14122

Table 4.3: Values used in the parameters of the potentials shown in Fig. (4.2)

that not all the chosen values, which are outside the restrictions, will give a trend like the one shown in this part. There will be combinations of values in the parameters for which the behavior obtained has a bad approximation towards the red line. In addition to this, it was possible to determine that in some cases, small variations in the chosen parameters can generate meaningless spectra, with chaotic behaviors.

4.2.2 Numerical analysis of the chaotic potential with a step with a combination between values that are outside and inside the limits

An interesting case that can be studied are the scalar spectra that can be presented if combinations of values that are inside and outside the limits are chosen.

Figure (4.3) uses the parameters shown in Table (4.4). From this illustration we can already determine that an $m = 7.5 \times 10^{-6} M_{pl}$ shifts the spectrum in the vertical direction and better fits the trend towards the red line. On the other hand, it is evident that the wave number and the number of oscillations are different in both cases; this case will be analyzed later. Then, there can be combinations of potential parameter values, inside and outside of the established restrictions, for which the potential oscillates and has a good approximation towards the red line.

4.2.3 Numerical analysis of the chaotic potential with the lower and upper limit values

From these spectra we can only emphasize what was mentioned above regarding m , which helps to obtain a better adjustment towards the red line by displacing it vertically (see Fig. (4.4)). This is a good moment to mention that the ranges shown in Table (4.2) do not guarantee that all the possible parameter combinations generate oscillations and good approximations to the red line, but rather that within these limitations, the best fit to the temperature spectrum at small angular momentum, obtained observationally, will be found.

4.2.4 Numerical analysis of the potential with values within the limits

It is important to be able to understand the behavior of all parameters that conform the step potential when they take different values. Thus, in this section we analyze the changes made to c , ϕ_{step} and d when their values vary smoothly.

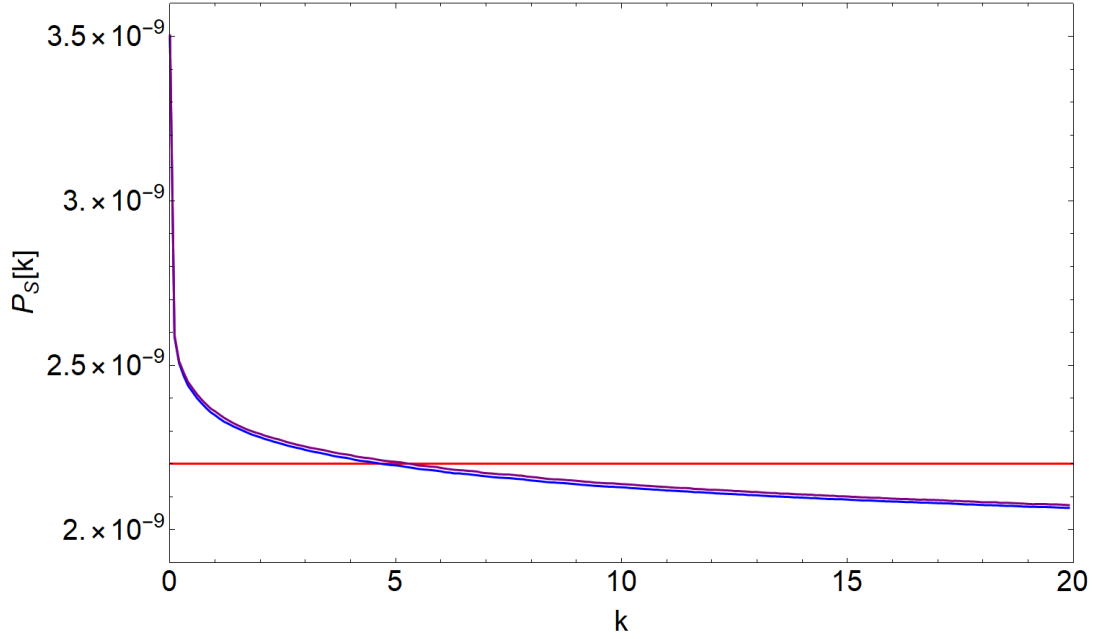


Figure 4.2: Scalar power spectrum for values of c , ϕ_{step} and d that are outside the limits established in Table (4.2). The values considered for the blue color spectrum are above the limits, while for the purple color spectrum the values of the parameters are below the restrictions.

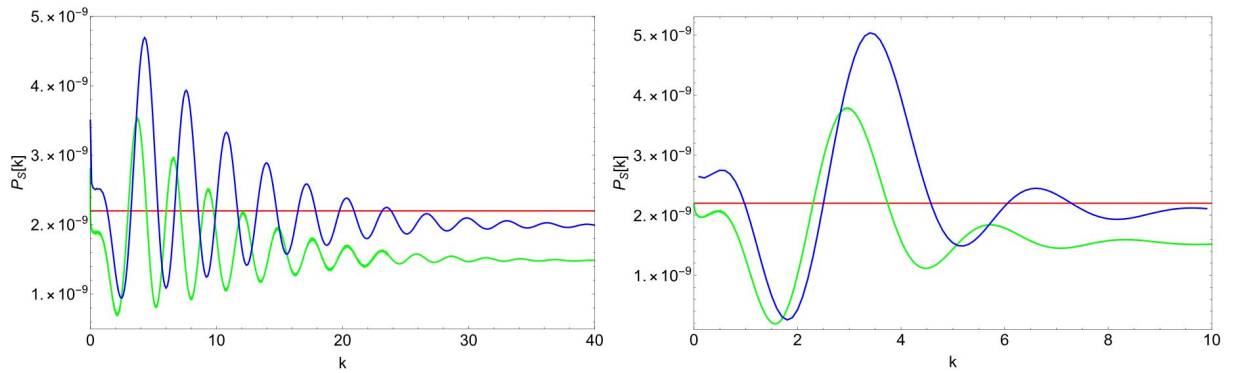


Figure 4.3: Scalar power spectrum for combinations of values that are inside and outside the limits. **Left:** where c is the only parameter whose value is outside the limits. **Right:** choosing c and d with values outside the restrictions. In both cases the oscillations with blue color have a value of $m = 7.5 \times 10^{-6} M_{pl}$ while for the oscillations with green color a value $m = 6.5 \times 10^{-6} M_{pl}$ was used. The red line shows the final trend that a model must follow in order to be considered valid.

Model	Parameter	Blue Graph	Green Graph
Chaotic Model with a step (Left)	$m[M_{pl}]$	7.5×10^{-6}	6.5×10^{-6}
	ϕ_0	15.4500	15.4500
	c	0.00200	0.00200
	ϕ_{step}	14.0900	14.0900
	d	0.01000	0.01000
Power law case	n_s	0.96069	0.96293
	r	0.14102	0.14142
Chaotic Model with a step (Right)	$m[M_{pl}]$	7.5×10^{-6}	6.5×10^{-6}
	ϕ_0	15.4500	15.4500
	c	0.01000	0.01000
	ϕ_{step}	14.0900	14.0900
	d	0.05000	0.05000
Power law case	n_s	0.96128	0.96345
	r	0.14097	0.14135

Table 4.4: Parameters used to obtain the figure of the power spectrum in Fig. (4.3), with m being the only one quantity that varies in the graph on the left and right. The numbers in bold represent the chosen quantities that are outside the limits.

Model	Parameter	Blue Graph	Purple Graph
Chaotic Model with a step (Lower Limit)	$m[M_{pl}]$	7.5×10^{-6}	6.5×10^{-6}
	ϕ_0	15.45000	15.45000
	c	0.01300	0.01300
	ϕ_{step}	13.0000	13.0000
	d	0.01000	0.01000
Power law case	n_s	0.95945	0.96099
	r	0.14119	0.14160
Chaotic Model with a step (Upper Limit)	$m[M_{pl}]$	7.5×10^{-6}	6.5×10^{-6}
	ϕ_0	15.4500	15.4500
	c	0.01700	0.01700
	ϕ_{step}	15.0000	15.0000
	d	0.04000	0.04000
Power law case	n_s	4.59749	31.35950
	r	1.46745	1.95785

Table 4.5: Upper and lower limit of the potential parameters calculated with the Markov Chain Monte-Carlo method. The values of n_s and r were obtained for both limits

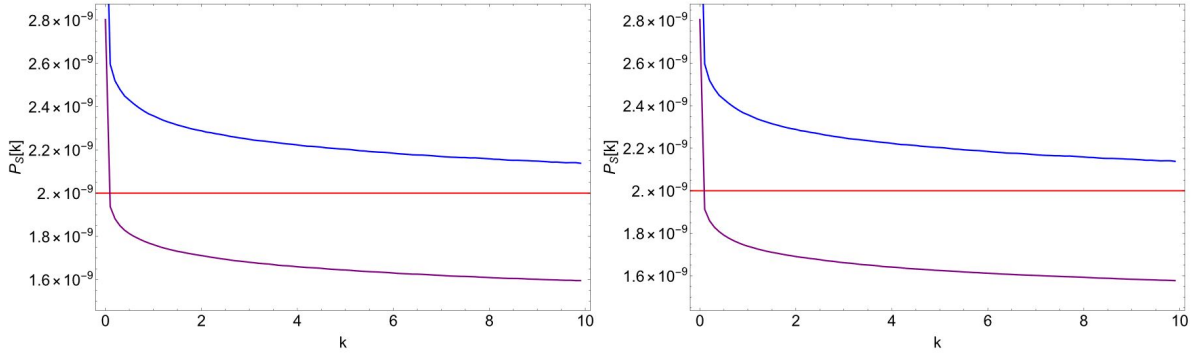


Figure 4.4: Scalar spectrum for the chaotic potential with the parameters defined in Table (4.5). **Left:** lower limit. **Right:** upper limit. In both cases, m is the only parameter varied in the blue ($m = 7.5 \times 10^{-6}$) and purple ($m = 6.5 \times 10^{-6}$) graphs. As in the previous cases, the red line represents the trend that the studied potential should follow.

Model	Parameter	Green Graph	Purple Graph	Blue Graph
Chaotic Model with a step	$m[M_{pl}]$	7.5×10^{-6}	7.5×10^{-6}	7.5×10^{-6}
	ϕ_0	15.4500	15.4500	15.4500
	c	0.01400	0.01500	0.01600
	ϕ_{step}	14.0000	14.0000	14.0000
	d	0.03000	0.03000	0.03000
Power law case	n_s	0.96185	0.96213	0.96178
	r	0.142156	0.14099	0.14099

Table 4.6: Values considered for the parameters of the step potential. The variation occurs over the value c , while the rest of the quantities remain constant. The power law cases (n_s and r) were calculated

Varying the parameter c

If we consider different values of c , keeping the rest of the parameters constant (see Table 4.6). In Figure (4.5) we can observe how the peaks of the oscillations produced in the spectrum increase in magnitude when c takes larger values. The number of oscillations produced does not change and at the end they will all converge onto a single line whose approximation is good with respect to the red line. This was to be expected, since the values considered are within the limits, in all cases.

Varying the parameter ϕ_{step}

For this case, we vary ϕ_{step} with the values shown in Table (4.7). The wavenumber for these spectra ranges from $k = 0$ to $k = 10$.

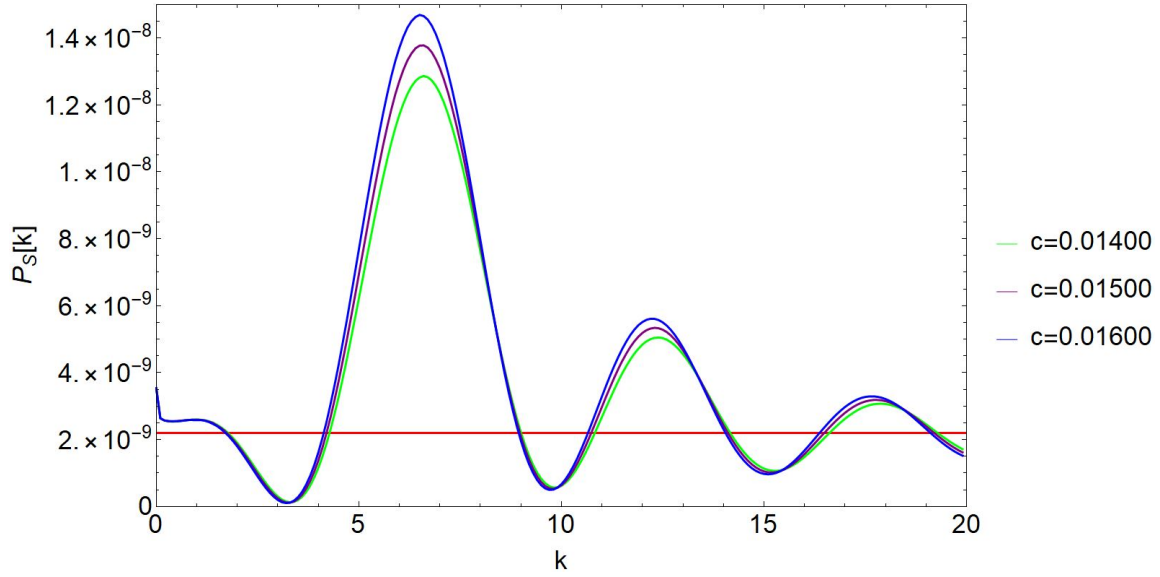


Figure 4.5: Scalar power spectrum for different values of c . The oscillatory behavior in this case shows an increase in the amplitude of the wave as c increases as well.

Model	Parameter	Green Graph	Purple Graph	Blue Graph
Chaotic Model with a step	$m[M_{pl}]$	7.5×10^{-6}	7.5×10^{-6}	7.5×10^{-6}
	ϕ_0	15.4500	15.4500	15.4500
	c	0.01500	0.01500	0.01500
	ϕ_{step}	13.5000	14.2000	14.5000
	d	0.02000	0.02000	0.02000
Power law case	n_s	0.95971	0.96153	0.96111
	r	0.14118	0.14104	0.14102

Table 4.7: Values considered for the step potential parameters. The variation of ϕ_{step} between the second and third value is smaller in relation to the first.

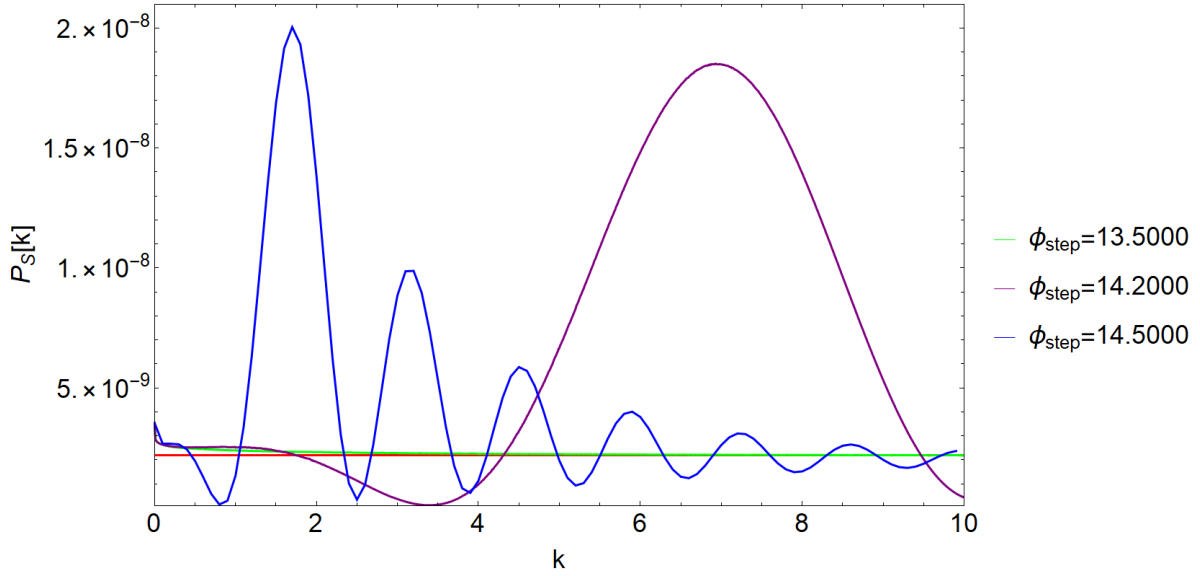


Figure 4.6: Scalar power spectrum for different values of ϕ_{step} . The oscillatory frequency of the blue color spectrum is greater than purple and green color spectra.

The wavelengths observed in the spectra decrease when the ϕ_{step} variable increases its value. The values considered for the purple and blue color spectra only differ in 0.3. However, the oscillations they produce are completely different, since the frequency of the blue color spectrum observed in Figure (4.6), is much higher than the frequency of the purple color spectrum. For the green color spectrum no type of oscillation is observed, its behavior is very similar to that obtained for the chaotic potential without the step in this range of k .

Varying the parameter d

For the last case that we studied on data variation in the parameters, the quantities shown in Table (4.8) were used.

In the spectra for this case, shown in Fig. (4.7), it can be observed how the behavior of the oscillations is contrary to the cases analyzed previously. That is, we can see how an increase in the value of the parameter d decreases both the amplitude and the frequency of each oscillation.

Best fit in potential parameters

Finally, after having made a large number of combinations between the parameters c , ϕ_{step} and d , it was possible to find a combination, see Table (4.9), whose scalar power spectrum fits with good precision for the data obtained from space telescopes with respect to the temperature spectrum. In the section 3.3 we saw what this fit looks like for angular momentum near to $l = 22$ and $l = 40$. That is, the values of the parameters used for this fit show a good approximation at these small angular momentum in the temperature spectrum. This occurs because our scalar

Model	Parameter	Green Graph	Purple Graph	Blue Graph
Chaotic Model with a step	$m[M_{pl}]$	7.5×10^{-6}	7.5×10^{-6}	7.5×10^{-6}
	ϕ_0	15.4500	15.4500	15.4500
	c	0.01200	0.01200	0.01200
	ϕ_{step}	14.0900	14.0900	14.0900
	d	0.02000	0.02500	0.03500
Power law case	n_s	0.96110	0.96131	0.96164
	r	0.14104	0.14104	0.14100

Table 4.8: Different values considered for parameter d . The quantities n_s and r obtained for this case are shown

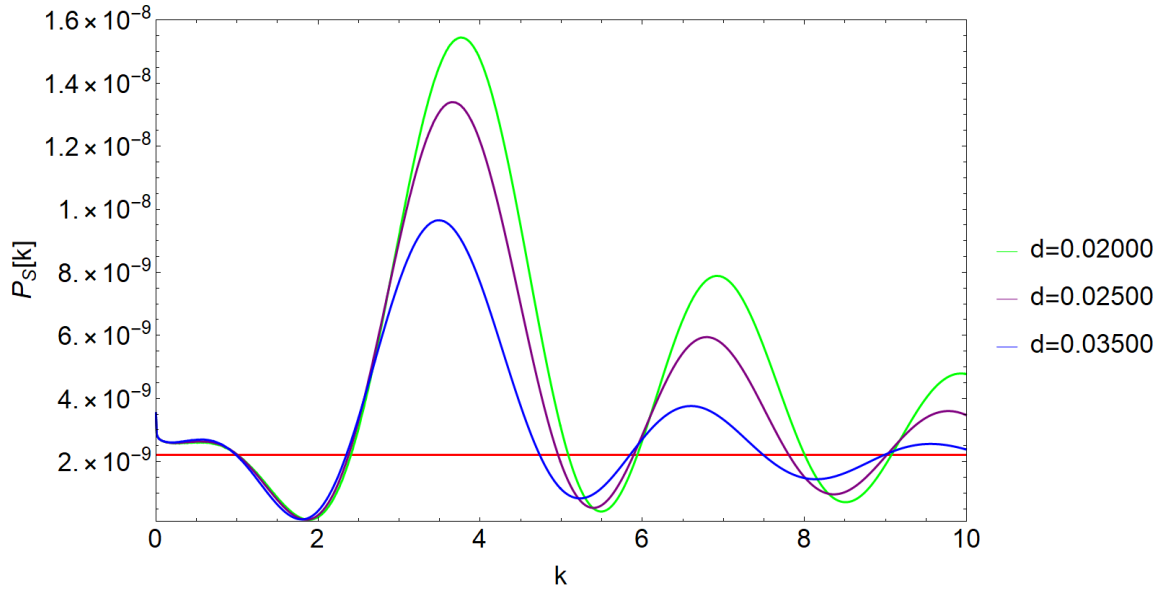


Figure 4.7: Spectrum of scalar powers for different values of d . The behavior of these oscillations looks contrary to those obtained by the previous spectra.

Model	Parameter	Value
Chaotic Model with a step	$m[M_{pl}]$	7.5×10^{-6}
	ϕ_0	15.4500
	c	0.01600
	ϕ_{step}	14.6700
	d	0.03110
Power law case	n_s	0.98523
	r	0.13959

Table 4.9: Values of the parameters that best fit the observational data from space telescopes. The quantities n_s and r obtained for this fit are shown.

Parameter	Symbol	Theoretically	Observationally	Error (%)
Scalar spectral index	n_s	0.98523	0.9649	2.10695
Tensor-to-scalar ratio	r	0.13959	0.11000	26.9000

Table 4.10: Experimental and theoretical values obtained for n_s and r .

power spectrum, as you can see in the Fig. (4.8), meets the requirements that have been mentioned throughout this work. In addition, the good approximation obtained can be sustained because the values obtained for n_s and r are very close to those obtained observationally. This did not occur for most of the cases analyzed previously, where the results obtained for the power law case were even far from the limits established in Table (4.2).

With all these calculations obtained, we can compare the values of the power law case obtained theoretically with the best fit, to the experimental values of the Planck telescope that are shown in the Table (4.10). The errors obtained in n_s and r for this fit are small. The cases analyzed at the beginning of this section show considerably high errors, far from the observational values obtained by space telescopes.

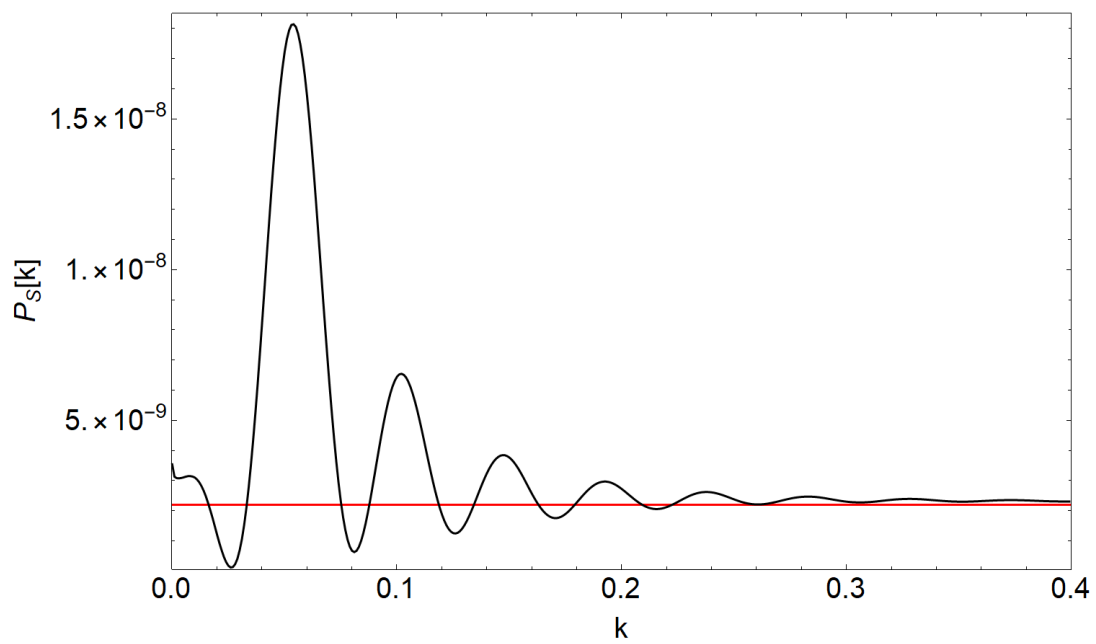


Figure 4.8: The scalar power spectrum of the best fit found for the chaotic potential with a step. The graph shows oscillations and its final value tends to have a value of 2.2×10^{-9} . The range of the wavenumber is smaller in relation to the previous cases.

Chapter 5

Conclusions & Outlook

In this work the chaotic potential with a step was analyzed numerically. We first present the theoretical background by mentioning the horizon and flatness problems whose solutions gave rise to the theory of cosmic inflation. From the study of cosmological disturbances, which give rise to the structure of the Universe, the Mukhanov-Sasaki equation is obtained. The chaotic potential and the step potential were examined. The product of these two potentials gave us as a result a new potential whose objective is to obtain the scalar power spectrum with oscillations, in order to obtain a temperature spectrum with a good approximation with respect to the data collected by telescopes such as the Planck or the WMAP-9. For the numerical analysis of this potential with a step, Table (4.2) was used, which shows the range of values that the height (c), location (ϕ_{step}), and width (d) can have so that the scalar spectrum shows oscillations. Once the analysis on the parameters was carried out, considering combinations of values that are outside, inside and in the limits, it was possible to determine the behavior that each of the variables has when their values vary. It was observed how all the spectra obtained have a better approximation for an inflaton mass $m = 7.5 \times 10^{-6} M_{pl}$. As expected, the approximations and oscillatory behaviors obtained for the combinations made between the variables that are outside the range shown above, do not fit the experimental data correctly. This also happens for the potential quantities n_s and r that were obtained. All the cases studied within the established limits, present oscillations and a good approximation towards the value 2.2×10^{-9} . However, there will only be a combination of values, within limits shown in Table (4.2), that best fit the data from space telescopes, this for small multipole moments.

The analysis done on each of the variables shows how the amplitude of the oscillations increases when c takes larger values. In the case of the ϕ_{step} parameter, the frequencies that the oscillations present are greater as the value of the variable increases. On the other hand, the variable d presents a behavior opposite to that shown by c and ϕ_{step} . Fig. (4.8) shows the scalar power spectrum that best fits these data. Unlike the oscillations obtained for the other cases studied, we can notice how these are produced at lower wavenumbers.

For future studies with this potential, this work will be helpful to understand the values that the variables c , ϕ_{step} , and d must have, so that the spectrum of scalar powers has a good fit with respect to the new observational data that are obtained.

Appendix A

Mathematica code to compute the scalar power spectrum and the values for n_s and r

```
ClearAll["Global`*"]

\[Phi]s := 14.8
\[Phi]0 := 16.5
m := 6.7375 10^(-6)
c := 0.0018
d := 0.022
\[Phi]end := 1.41421
V[t_] := 1/2 m^2 \[Phi][t]^2 (1 + c Tanh[(\[Phi][t] - \[Phi]s)/d])
Vp[t_] := D[V[t], {\[Phi][t], 1}]
(*\[Phi]sr, asr*)
solsr = NDSolve[{3 a'[t]/a[t] \[Phi]'[t] + Vp[t] == 0,
  a'[t] == a[t] Sqrt[1/3 V[t]], \[Phi][0] == \[Phi]0,
  a[0] == 1}, {\[Phi], a}, {t, -42000, 2.99 10^6},
  MaxSteps -> 100000, AccuracyGoal -> 10];
asr[t_] := (a /. First[solsr])[t]
\[Phi]sr[t_] := (\[Phi] /. First[solsr])[t]
\[Phi]srp[t_] = D[\[Phi]sr[t], {t, 1}];
(*\[Phi], a*)
solex = NDSolve[{\[Phi]t''[t] + 3 at'[t]/at[t] \[Phi]t'[t] +
  m^2 (1 + c Tanh[-\[Phi]s + \[Phi]t[t])/d] \[Phi]t[t] + (
  c m^2 Sech[-\[Phi]s + \[Phi]t[t])/d]^2 \[Phi]t[t]^2)/(2 d) ==
```

```

0, at'[t] ==
at[t] Sqrt[
  1/3 (1/2 \[Phi]t'[t]^2 +
    1/2 m^2 \[Phi]t[t]^2 (1 +
      c Tanh[(\[Phi]t[t] - \[Phi]S)/d])), \[Phi]t[
0] == \[Phi]0, \[Phi]t'[0] == \[Phi]srp[0],
at[0] == 1}, {\[Phi]t , at}, {t, -42000, 2.99 10^6},
MaxSteps -> 100000000, AccuracyGoal -> 10];
a[t_] := (at /. First[solex])[t]
pa[t_] := (at' /. First[solex])[t];
ppa[t_] := (at'' /. First[solex])[t];
pppa[t_] := (at''' /. First[solex])[t];
\[Phi][t_] := (\[Phi]t /. First[solex])[t];
p\[Phi][t_] := (\[Phi]t' /. First[solex])[t];
pp\[Phi][t_] := (\[Phi]t'' /. First[solex])[t];
ppp\[Phi][t_] := (\[Phi]t''' /. First[solex])[t];
H[t_] := pa[t]/a[t]
z[t_] := (a[t] p\[Phi][t])/H[t]
tend = t /. FindRoot[\[Phi][t] == \[Phi]end, {t, 2.4 10^6}];
Efolds = Log[a[tend]/a[0]];
pH[t_] = D[H[t], t];
z[t_] := ((a[t])^2 p\[Phi][t])/pa[t];
pz[t_] :=
  a[t] (p\[Phi][t] (2 - (a[t] ppa[t])/pa[t]^2) + (a[t] pp\[Phi][t])/
    pa[t])
ppz[t_] :=
  2 pa[t] p\[Phi][t] + (2 a[t]^2 p\[Phi][t] ppa[t]^2)/pa[t]^3 +
  4 a[t] pp\[Phi][t] - (
  a[t]^2 (2 ppa[t] pp\[Phi][t] + p\[Phi][t] pppa[t]))/pa[t]^2 + (
  a[t] (-2 p\[Phi][t] ppa[t] + a[t] ppp\[Phi][t]))/pa[t]
Plot[\[Phi][t] - \[Phi]end, {t, 0, 3 10^6}, PlotRange -> All]
tend

prere[k_] :=
NDSolve[{l''[t] + l'[t] H[t] + l[t] (k/a[t])^2 == 0,
  l[tbuch[k]] == Re[uini[k, tbuch[k]]],
  l'[tbuch[k]] == Re[diffuini[k, tbuch[k]]]}, {l, l'}, {t, tbuch[k],
  tini[k]}, MaxSteps -> Infinity, StartingStepSize -> .0001,

```

```

    MaxStepSize -> 10, InterpolationOrder -> All];
re[k_] :=
  NDSolve[{u''[t] + u'[t] H[t] + u[t] rhsScalar[k, t] == 0,
    u[tini[k]] == Rationalize[1 /. First[prere[k]]][tini[k]], 0},
    u'[tini[k]] == Rationalize[1' /. First[prere[k]]][tini[k]], 0}},
  u, {t, tini[k], 3 hc[k]}, MaxSteps -> Infinity,
  StartingStepSize -> .001, MaxStepSize -> 10,
  InterpolationOrder -> All];
preim[k_] :=
  NDSolve[{g''[t] + g'[t] H[t] + g[t] (k/a[t])^2 == 0,
    g[tbuch[k]] == Im[uini[k, tbuch[k]]],
    g'[tbuch[k]] == Im[diffuini[k, tbuch[k]]]}, {g, g'}, {t, tbuch[k],
    tini[k]}, MaxSteps -> Infinity, StartingStepSize -> .0001,
  MaxStepSize -> 10, InterpolationOrder -> All];
im[k_] :=
  NDSolve[{v''[t] + v'[t] H[t] + v[t] rhsScalar[k, t] == 0,
    v[tini[k]] == Rationalize[(g /. First[preim[k]]][tini[k]], 0],
    v'[tini[k]] == Rationalize[(g' /. First[preim[k]]][tini[k]], 0]},
  v, {t, tini[k], 3 hc[k]}, MaxSteps -> Infinity,
  StartingStepSize -> .001, MaxStepSize -> 10,
  InterpolationOrder -> All];
x[k_] := u /. First[re[k]]
y[k_] := v /. First[im[k]]
(*Tensor*)
prere2[k_] :=
  NDSolve[{l2''[t] + l2'[t] H[t] + l2[t] (k/a[t])^2 == 0,
    l2[tbuch[k]] == Re[uini[k, tbuch[k]]],
    l2'[tbuch[k]] == Re[diffuini[k, tbuch[k]]]}, {l2, l2'}, {t,
    tbuch[k], tini[k]}, MaxSteps -> Infinity,
  StartingStepSize -> .0001, MaxStepSize -> 10,
  InterpolationOrder -> All];
re2[k_] :=
  NDSolve[{u2''[t] + u2'[t] H[t] + u2[t] rhsTensor[k, t] == 0,
    u2[tini[k]] == Rationalize[(l2 /. First[prere2[k]])[tini[k]], 0],
    u2'[tini[k]] ==
    Rationalize[(l2' /. First[prere2[k]])[tini[k]], 0]},
  u2, {t, tini[k], 3 hc[k]}, MaxSteps -> Infinity,
  StartingStepSize -> .001, MaxStepSize -> 10,

```

```

InterpolationOrder -> All];
preim2[k_] :=
NDSolve[{g2''[t] + g2'[t] H[t] + g2[t] (k/a[t])^2 == 0,
g2[tbuch[k]] == Im[uini[k, tbuch[k]]],
g2'[tbuch[k]] == Im[diffuini[k, tbuch[k]]]}, {g2, g2'}, {t,
tbuch[k], tini[k]}, MaxSteps -> Infinity,
StartingStepSize -> .0001, MaxStepSize -> 10,
InterpolationOrder -> All];
im2[k_] :=
NDSolve[{v2''[t] + v2'[t] H[t] + v2[t] rhsTensor[k, t] == 0,
v2[tini[k]] == Rationalize[(g2 /. First[preim2[k]])[tini[k]], 0],
v2'[tini[k]] ==
Rationalize[(g2' /. First[preim2[k]])[tini[k]], 0]},
v2, {t, tini[k], 3 hc[k]}, MaxSteps -> Infinity,
StartingStepSize -> .001, MaxStepSize -> 10,
InterpolationOrder -> All];
x2[k_] := u2 /. First[re2[k]]
y2[k_] := v2 /. First[im2[k]]

PS[k_] :=
k^3/(2 Pi^2 (z[3 hc[k]])^2) Abs[(x[k])[3 hc[k]] + I (y[k])[3 hc[k]]]^2
PT[k_] :=
k^3/(2 Pi^2 (a[3 hc[k]])^2)
Abs[(x2[k])[3 hc[k]] + I (y2[k])[3 hc[k]]]^2
nS[k_] := 1 + k/PS[k] (PS[k + h2] - PS[k - h2])/(2 h2)
r[k_] := 8 PT[k]/PS[k]

data1 = OpenWrite[
"G:\\My Drive\\TRABAJO DE TITULACIÓN\\Titulación \\
I\\Mathematica\\Séptimos Valores C= 0.012 d= 0.004\\Data C=0.012 \\
d=0.004 - Proagation k+0.01 from 0.0001-10.0000.txt",
FormatType -> OutputForm]; For[k = 7.9891, k < 10, k = k + 0.01,
Write[data1, k, " ", CForm[PS[k]]]
Close[data1];

```

Bibliography

- [1] Vázquez, J. A.; Padilla, L. E.; Matos, T. Inflationary cosmology: from theory to observations. *EDUCATION* **2020**, *17*, 73–91.
- [2] Baumann, D. Cosmological inflation: Theory and observations. *Advanced Science Letters* **2009**, *2*, 105–120.
- [3] Hazra, D. K.; Aich, M.; Jain, R. K.; Sriramkumar, L.; Souradeep, T. Primordial features due to a step in the inflaton potential. *Journal of Cosmology and Astroparticle Physics* **2010**, *2010*, 008.
- [4] Tsujikawa, S. Introductory review of cosmic inflation. **2003**,
- [5] de Boer, J.; Hartong, J.; Obers, N.; Sybesma, W.; Vandoren, S. Perfect fluids. *SciPost Physics* **2018**, *5*, 003.
- [6] Guth, A. H. Inflation and eternal inflation. *Physics Reports* **2000**, *333*, 555–574.
- [7] Lake, K. The flatness problem and Λ . *Physical review letters* **2005**, *94*, 201102.
- [8] Davis, T. M.; Lineweaver, C. H. Expanding confusion: common misconceptions of cosmological horizons and the superluminal expansion of the universe. *Publications of the Astronomical Society of Australia* **2004**, *21*, 97–109.
- [9] Fixsen, D. The temperature of the cosmic microwave background. *The Astrophysical Journal* **2009**, *707*, 916.
- [10] Linde, A. *Particle physics and inflationary cosmology*; CRC press, 1990; Vol. 5.
- [11] Liddle, A. R.; Lyth, D. H. *Cosmological inflation and large-scale structure*; Cambridge university press, 2000.
- [12] Lyth, D. H.; Liddle, A. R. *The primordial density perturbation: Cosmology, inflation and the origin of structure*; Cambridge University Press, 2009.
- [13] Muñoz, M. A. C. Perturbaciones en modelos cosmológicos inflacionarios. Ph.D. thesis, Universidad de Concepción, 2010.
- [14] Lyth, D. H. *Inflationary Cosmology*; Springer, 2008; pp 81–118.
- [15] Riotto, A. *Inflation and the theory of cosmological perturbations*; 2003.

-
- [16] Ryden, B. *Introduction to cosmology*; Cambridge University Press, 2017.
- [17] Raine, D.; Thomas, T. *An introduction to the science of cosmology*; CRC press, 2018.
- [18] Tapia, T.; Rojas, C. *Scalar Cosmological Perturbations*; 2020.
- [19] Padmanabhan, T. *Structure formation in the universe*; Cambridge university press, 1993.
- [20] Orozco Sánchez, E. A. Study of the Starobinsky inflationary model into the slow-roll approximation. B.S. thesis, Universidad de Investigación de Tecnología Experimental Yachay, 2021.
- [21] Dodelson, S. *Modern cosmology*; Elsevier, 2003.
- [22] Adams, J.; Cresswell, B.; Easther, R. Inflationary perturbations from a potential with a step. *Physical Review D* **2001**, *64*, 123514.
- [23] Deruelle, N.; Gundlach, C.; Polarski, D. On the quantization of perturbations in inflation. *Classical and Quantum Gravity* **1992**, *9*, 137–148.
- [24] Planck Collaboration, *et al.* Planck 2018 results. VI. Cosmological parameters. **2020**, *641*, A6.
- [25] Hinshaw, G.; Larson, D.; Komatsu, E.; Spergel, D. N.; Bennett, C.; Dunkley, J.; Nolte, M.; Halpern, M.; Hill, R.; Odegard, Nine-year Wilkinson Microwave Anisotropy Probe (WMAP) observations: cosmological parameter results. *The Astrophysical Journal Supplement Series* **2013**, *208*, 19.